3D U-SPATIAL STATISTICS APPLET: CASE STUDY IN TWO DISTINCT GOLD SYSTEMS IN THE EASTERN PONTIDES IN NE TÜRKİYE

A THESIS SUBMITTED TO
THE GRADUATE SCHOOL OF NATURAL AND APPLIED SCIENCES
OF
MIDDLE EAST TECHNICAL UNIVERSITY

BY

GÜNEŞ ERTUNÇ

IN PARTIAL FULFILLMENT OF THE REQUIREMENTS
FOR
THE DEGREE OF MASTER OF SCIENCE
IN
GEOLOGICAL ENGINEERING

SEPTEMBER 2023

Approval of the thesis:

3D U-SPATIAL STATISTICS APPLET: CASE STUDY IN TWO DISTINCT GOLD SYSTEMS IN THE EASTERN PONTIDES IN NE TÜRKİYE

submitted by **GÜNEŞ ERTUNÇ** in partial fulfillment of the requirements for the degree of **Master of Science in Geological Engineering Department, Middle East Technical University** by,

Prof. Dr. Halil Kalıpçılar
Dean, Graduate School of **Natural and Applied Sciences** _____

Prof. Dr. Erdin Bozkurt
Head of Department, **Geological Engineering** _____

Assist. Prof. Dr. Ali İmer
Supervisor, **Geological Engineering, METU** _____

Examining Committee Members:

Prof. Dr. A. Erhan Tercan
Mining Engineering, Hacettepe University _____

Assist. Prof. Dr. Ali İmer
Geological Engineering, METU _____

Prof. Dr. Kaan Sayıt
Geological Engineering, METU _____

Assoc. Prof. Dr. Sinan Akıska
Geological Engineering, Ankara University _____

Assist. Prof. Dr. Erkan Yılmazer
Geological Engineering, Aksaray University _____

Date: 11.09.2023

I hereby declare that all information in this document has been obtained and presented in accordance with academic rules and ethical conduct. I also declare that, as required by these rules and conduct, I have fully cited and referenced all material and results that are not original to this work.

Name, Surname: Güneş Ertunç

Signature :

ABSTRACT

3D U-SPATIAL STATISTICS APPLET: CASE STUDY IN TWO DISTINCT GOLD SYSTEMS IN THE EASTERN PONTIDES IN NE TÜRKİYE

Ertunç, Güneş
M.S., Department of Geological Engineering
Supervisor: Assist. Prof. Dr. Ali İmer

September 2023, 77 pages

Geochemical anomalies that develop around metallic mineralizations are directly linked to ore formation processes and play an important role in mineral exploration. In exploration geochemistry, a non-anomalous element concentration is referred to as the background value. Considering the practical implications in exploration, statistical methods have been utilized not only for assessing background concentrations, but also for the separation of geochemical anomalies from background.

The aim of this study is to determine the geochemical anomaly zones in two different Au mineralizations located in the Eastern Pontide Magmatic Belt in NE Anatolia which are of great importance in terms of regional metallogeny. For this purpose, 3D geochemical anomaly mapping was carried out with the U-Statistics methodology using drillhole databases.

In the Salınbaş Au prospect, located about 20 km SE of Artvin and representing a carbonate-replacement type mineralization, anomaly zones were determined as isolated clusters with low lateral continuity. It is thought that this distribution is particularly controlled by the shallowly dipping lithological contact in the study area.

Additionally, the sporadic distribution of the anomaly zones is probably due to the karst development along which ore precipitation occurred.

At the Taç project, which is an intermediate-sulfidation epithermal type mineralization located approximately 4 km SW of Yusufeli (Artvin), horizontal and vertical continuity of the anomaly zone is evident. The domain of vertical continuity in the prospect area is controlled by vertical structures that feed the main ore zone. However, ore continuity decreases outside of this zone.

The 3D U-Statistics models established in Salınbaş and Taç revealed the differences in the formation processes of different types of Au mineralizations in these areas. With this study, a 3D geochemical anomaly mapping was carried out for the first time in Türkiye by creating a GUI software.

Keywords: U-Stats, Matlab GUI, Geochemical anomaly, Carbonate-replacement, Epithermal gold

ÖZ

3 BOYUTLU U-İSTATİSTİK PROGRAMI: DOĞU PONTİDLER (KD TÜRKİYE)'DE İKİ FARKLI ALTIN YATAĞINDA DURUM ÇALIŞMASI

Ertunç, Güneş
Yüksek Lisans, Jeoloji Mühendisliği Bölümü
Tez Yöneticisi: Dr. Öğr. Üyesi. Ali İmer

Eylül 2023 , 77 sayfa

Metalik maden oluşumlarının çevresinde gelişen jeokimyasal anomaliler cevher oluşum süreçleri ile doğrudan bağlantılıdır ve maden aramada önemli bir rol oynarlar. Anomali olmayan jeokimyasal veriler, arka plan değeri olarak değerlendirilmektedir. Endüstri pratiğinden elde edilen çıkarımlar göz önüne alındığında, istatistiksel yöntemler yalnızca arka plan konsantrasyonlarını değerlendirmek için değil, aynı zamanda jeokimyasal anomalilerin jeokimyasal arka plandan ayrılması için de kullanılmıştır.

Bu çalışmada KD Anadolu'da bulunan Doğu Pontid Magmatik Kuşagı'nda yer alan ve bölgesel metalojeni açısından büyük önem taşıyan iki farklı Au cevherleşmesinde jeokimyasal anomali zonlarının belirlenmesi amaçlanmıştır. Bu doğrultuda sondaj veritabanları kullanılarak U-Statistics yöntemi ile 3B jeokimyasal anomali haritalandırılması yapılmıştır.

Artvin'in yaklaşık 20 km güneydoğusunda yer alan ve karbonat ornatma tipi bir cevherleşmeyi temsil eden Salınbaş Au prospektinde anomali zonları yanal devamlılığı

düşük ve birbirinden ayrık kümeler şeklinde belirlenmiştir. Bu dağılımın özellikle sahadaki sığ açılı litolojik dokanak tarafından kontrol edildiği düşünülmektedir. Ayrıca, zonların ayrık yapısı olasılıkla cevherin içerisine girdiği karstik boşluklardan kaynaklanmaktadır.

Artvin'in Yusufeli ilçesinin yaklaşık 4 km güneybatısında yer alan ortaç-sülfidasyon epitermal tipteki Taç sahasında ise anomali zonunda yatay ve düşeyde devamlılık söz konusudur. Sahada düşey devamlılığın olduğu bölge ana cevher zonunu besleyen dik açılı yapılarla kontrol edilmektedir. Ancak bu zonun dışına çıkıldığında, devamlılık etkisini yitirmektedir.

Salınbaş ve Taç sahalarında ortaya çıkan 3B U-Statistics modelleri iki sahadaki farklı Au cevherleşmesi tiplerinin oluşum süreçlerinden kaynaklı farklılıklarını açıkça ortaya koymuştur. Bu çalışmayla birlikte Türkiye'de ilk defa 3B bir jeokimyasal anomali haritalandırılması, bir bilgisayar programı kullanıcı arayüzü oluşturularak gerçekleştirilmiştir.

Anahtar Kelimeler: U-Stats, Matlab GUI, Jeokimyasal anomali, Karbonat-onartma, Epitermal altın

"I do not fear computers. I fear the lack of them."

-Isaac Asimov

ACKNOWLEDGMENTS

First of all, I would like to express my gratitude to my advisor Dr Ali İMER, whom I have witnessed many times doing his job with great enthusiasm. He has truly been an inspiration. Thank you.

I would also like to thank all jury members, Dr A. Erhan TERCAN, Dr Kaan SAYIT, Dr Sinan AKISKA and Dr Erkan YILMAZER. They contributed greatly to the final version of the thesis with their valuable feedback.

Special thanks to Santral Madencilik and Zenit Madencilik Dr Arman KOÇAL and Derya BAL for the data sharing. Also, thanks to Ariana Resources Ankara office for the fruitful discussions with Berkin UĞURLU and his team.

I would like to thank to those who created METU thesis LaTeX template from past to present and/or contributed to its updates. This really saved me a lot of time.

I dedicate this thesis to my family. I love you deeply with all my heart. My wife Funda, and my son Ali Çağan.

TABLE OF CONTENTS

ABSTRACT v

ÖZ vii

ACKNOWLEDGMENTS x

TABLE OF CONTENTS xi

LIST OF TABLES xiii

LIST OF FIGURES xiv

LIST OF ABBREVIATIONS xviii

CHAPTERS

1 INTRODUCTION 1

1.1 Purpose and Scope 2

1.2 Geographic Location and Geology of the Study Areas 4

1.3 Previous Studies 11

1.4 Structure of the Thesis 13

2 METHODOLOGY 15

3 U-STATS GUI: DEMO, CHENG ET AL. 1996 17

3.1 Sample Selection Strategy 19

3.2 Results 21

3.3 Re-run 22

3.3.1 A1 anomaly zone 24
3.3.2 A2 anomaly zone 25
4 U-STATS GUI: 2D 27
4.1 Data Import 27
4.2 Target Locations 28
4.3 Run and Results 29
5 U-STATS GUI: 3D 37
5.1 Database Import 37
5.2 Base Map 42
5.3 Digital Elevation Model Import 44
5.4 Target Locations 45
5.5 Search Ellipsoid 46
5.6 Run 47
5.7 Results 47
6 CASE STUDIES 49
6.1 Exploratory Data Analysis 49
6.2 Case Study: Salınbaş Mineralization 56
6.3 Case Study: Taç Mineralization 63
7 DISCUSSION, CONCLUSIONS, AND FUTURE WORK 69
REFERENCES 73

LIST OF TABLES

TABLES

Table 6.1 Descriptive statistics of Au (ppm) from both mineralizations. 52

Table 6.2 Results comparison of different multipliers of standard deviations in Salınbaş mineralization 61

Table 6.3 Results comparison of different multipliers of standard deviations in Taç mineralization 67

LIST OF FIGURES

FIGURES

Figure 1.1 Geologic map of the study area showing the distribution of magmatic hydrothermal mineral occurrences, lithologies, and the Hod gold corridor (bold dashed line). Modified from Rabayrol et al., 2023 5

Figure 1.2 Google Earth image of the Taç field and gold mineralization view in the field, (b) General view of the mineralization (photo faces north-northwest) 6

Figure 1.3 Google Earth image of the Taç field and gold mineralization view in the field, (b) General view of the mineralization (photo faces north-northwest) 7

Figure 1.4 Representative drill core photos of Taç Au mineralization. A: Semi-massive sulfide ore containing high grade Au (approximately 900 g/t) in pyrite-chalcopyrite mineralization. B: Characteristic siliceous breccia vein containing >5 g/t Au. C: Pyritic stockwork breccia vein. All cores are in HQ diameter. 8

Figure 1.5 Microphotographs of Cu Au mineralized samples from Taç. All photographs are reflected plane-polarized light images. Abbreviations: cpy=chalcopyrite, gn= galena, py=pyrite, rut=rutile, sph=sphalerite, and tet=tetrahedrite 9

Figure 1.6 Microphotographs of common ore textures from Taç. A: Quartz-sulfide stockwork veinlet in argillic altered andesite lava. B-C: Crustiform banded quartz-sulfide veins cross-cutting stockwork veinlets. D: Breccia vein consisting of mineralized siliceous vein clasts surronded by carbonate matrix. E: Intensely deformed siliceous breccia vein. F: Brecciated and argillic altered andesite. All photographs are transmitted, cross-polarized light images. Abbreviations: carb=carbonate, kaol=kaolinite, qz:Quartz, sulf=Sulfide 10

Figure 1.7 Map of the Ardala-Salınbaş area showing the distribution of plagioclase-acicular-hornblende magnetite bearing porphyritic intrusions (light pink with large crosses) in a rough circular pattern around the central Ardala Porphyry swarm (magenta). The red lines show a possible circular pattern to the plagioclase-acicular-hornblende magnetite bearing porphyritic intrusions distribution with a 5km diameter. The topographically higher ground to the SE, has preserved the flanking Avicular Formation (khaki spotty rock), which possibly erupted from the core of this circular intrusive complex. Modified from Groves et al., 2017 12

Figure 3.1 U-Stats GUI main window, Demo selection 17

Figure 3.2 U-Stats GUI Demo: Main window 18

Figure 3.3 U-Stats GUI Demo: Histogram of raw data 18

Figure 3.4 U-Stats GUI Demo: Base map 19

Figure 3.5 Geometric and angular parameters of ellipse and ellipsoid 20

Figure 3.6 Samples around in ellipsoid (included: green dots, excluded: red dots) 20

Figure 3.7 U-Stats (U^*) values 21

Figure 3.8 Histogram of U^* 22

Figure 3.9 Result plots 23

Figure 3.10 Re-run screen 24

Figure 3.11 Result plots: A1 anomaly zone 25

Figure 3.12 Result plots: A2 anomaly zone 26

Figure 4.1 U-Stats GUI main window: 2D selection 27

Figure 4.2 U-Stats GUI: 2D, data import 28

Figure 4.3 U-Stats GUI: 2D, target locations 29

Figure 4.4 U-Stats GUI: 2D, sample related plots 30

Figure 4.5 U-Stats GUI: 2D, search ellipse (in red) 31

Figure 4.6 U-Stats GUI: 2D, results related plots 32

Figure 4.7 U-Stats GUI: 2D, binary maps 33

Figure 4.8 Imported "2D.obj" in Surpac 2022 Refresh 3 35

Figure 5.1 U-Stats GUI main window, 3D selection 37

Figure 5.2 U-Stats GUI: 3D database import interface 38

Figure 5.3 Angles used in MCM calculation and curvature of the calculated path of borehole (dashed red line) 40

Figure 5.4 Borehole BH-118 41

Figure 5.5 Scatter plot, U-Stats GUI: 3D vs GEOVIA Surpac™ coordinates 42

Figure 5.6 U-Stats GUI: 3D, base map interface 43

Figure 5.7 U-Stats GUI: 3D, digital elevation model import interface 44

Figure 5.8 U-Stats GUI: 3D, target locations interface 45

Figure 5.9 U-Stats GUI: 3D, search ellipsoid interface 46

Figure 5.10 U-Stats GUI: 3D, progress bars 47

Figure 5.11 U-Stats GUI: 3D, results interface 48

Figure 6.1 Elevation map & borehole collars for a) Salınbaş and b) Taç projects 51

Figure 6.2 Histogram of Au (ppm) sample lengths from Salınbaş and Taç databases. 53

Figure 6.3 Histogram of Au(ppm) and log(Au(ppm)) from Salınbaş and Taç databases 54

Figure 6.4 Cumulative probability plots of Au (ppm) from Salınbaş (left) and Taç (right) databases. Plots were prepared both for raw and length-weighted data. 55

Figure 6.5 Salınbaş database import 56

Figure 6.6 U-Stats GUI: 3D, Salınbaş base map, color by Au (ppm) 57

Figure 6.7 3D digital elevation model import for Salınbaş 58

Figure 6.8 3D mesh grid for Salınbaş 58

Figure 6.9 Salınbaş search ellipsoid 59

Figure 6.10 U-Stats GUI: 3D, Salınbaş results 60

Figure 6.11 A: Plan view of geochemical anomaly zone output of 3D U-Stats, B: Au contours limestone contact. A and B are in same scale. B is modified from Groves et al., 2017 62

Figure 6.12 Taç database, alteration optional file import 63

Figure 6.13 U-Stats GUI: 3D, Taç base map 64

Figure 6.14 Taç search ellipsoid 65

Figure 6.15 U-Stats GUI: 3D, Taç results 66

LIST OF ABBREVIATIONS

2D	2 Dimensional
3D	3 Dimensional
ASCII	American Standard Code for Information Interchange
BLEG	Bulk leaching extractable gold
cos	cosine
DEM	Digital Elevation Model
DLS	Dogleg Severity
β	Dogleg Severity angle
ft	feet
Q1	first quartile
GUI	Graphical User Interface
Inf	Infinite
MAD	Median absolute deviation
MCM	Minimum Curvature Method
ppm	parts per million
PuOr	Purple Orange
PRGn	Purple Red Green
QR	Quick Response
RF	Ratio Factor
RdBu	Red Blue
RdYlBu	Red Yellow Blue
®	Registered trademark
Q2	second quartile
sin	sine

σ	standard deviation
Q3	third quartile
™	Trademark
URL	Uniform Resource Locator
U^*	U-Stats

CHAPTER 1

INTRODUCTION

Human impact on the environment is a never-ending issue. Changes to environment, populations, wildlife, and natural resources made directly or indirectly by humans. The impacts caused by humans are called anthropogenic impacts. Most of the time these impacts leave certain footprints in the nature; for example in rocks, top soil, plants, and water. These footprints are the anomalies and can be revealed by geochemical assessment of the attribute at interest. Etymologically anomaly is a descendant of the Greek word ἀνōμαλος (anōmalos), which means "uneven" or "irregular."

In this context, regularity in the nature can be defined as the geochemical background. According to Gough (1993) geochemical background is a natural value for a given medium not impacted by anthropogenic activities. On the other hand, exploration geochemists refer to a non-anomalous element concentration as a background (Plumlee, 1997). Considering the practical implications, the background value in exploration geochemistry is usually higher than in environmental geochemistry, because it may be influenced by both natural and anthropogenic concentrations. In the Dictionary of Geological Terms (Bates and Jackson, 1984) geochemical background is given as *"In geochemical prospecting, the range in values representing the normal concentration of a given element in a material under investigation such as rock, soil, plants, and water."*

There are two major methods used for assessing background concentrations: (1) Geochemical and (2) Statistical. The first method, also known as the empirical method, refers to studies of samples not affected by industrial activities or to relatively pristine/sterile sites (Crommentuijn et al., 2000; Baize and Sterckeman, 2001; Horckmans et al., 2005). These empirical studies are having subjective sample selection crite-

ria, high costs, and heavy laboratory workload. The second method, the statistical method has been used not only for assessing background concentrations, but also for the separation of geochemical anomalies from geochemical background. Majority of the statistical approaches are outlier detection and omitting that are considered to be anthropogenically influenced. These statistical methods for background assessments are well documented in (Matschullat et al., 2000).

For the statistical methodology the following assumptions are made for background and/or anomaly detection:

- The quality of the statistical analysis is based on quality of the input. The analyte should be analyzed without any significant loss or contamination, quantitatively.
- Majority of the geochemical prospecting data has spatial setting. Hence, by definition of regionalized variable (Matheron, 1971), geochemical background can only be derived for a defined spatial setting. This definition requires the proof of relative homogeneity, or domaining.
- Since the anthropogenic influence occurs by definition only as a contamination in the sense of a positive anomaly, the search for the geochemical background is reduced to the recognition of the relevant data sub-collective and its quantitative description.
- Assigning single values for a geochemical background is neither useful for the characterization of the background nor for the determination of an anthropogenic contamination, because single values do not yield information about the natural deviation. Consequently, a differentiated interpretation of results would be impossible. It is possible, however, to define upper limits for the background with a defined statistical reliability (Matschullat et al., 2000).

1.1 Purpose and Scope

The aim of the thesis is to apply the U-statistics method for three dimensional detection of gold anomalies on two separate gold-mineralized systems in the Eastern

Pontides in NE Türkiye. This is done through generation of a MATLAB algorithm. At the end of this study, a software is also developed, with a graphical user interface supporting both two-dimensional and three-dimensional solutions.

U-statistic (U-Stats) method has been introduced by Cheng et al., 1996 and as an effective method for differentiating anomalous samples from the background. In the past decade, it has been applied in 2D (Ghavami-Riabi et al., 2010, Ghannadpour et al., 2017 and 3D **Ghannadpour2016** limited to the vertical boreholes and without GUI.

In Türkiye, especially in the Au exploration literature, geochemical anomaly detection methods of companies in the form of in-house or third-party consultancy are generally limited to two dimensions and projections are created for the third dimension.

With this study, a comprehensive 3D study was carried out for the first time in Türkiye, and it can be emphasized that the project together with the 3D geochemical anomaly detection approach constitutes its novelty and broad impact.

The contribution and novelty of this study by means of U-Stats approach is that the search neighborhood can be adjusted for anisotropic cases by the user interface and the method is supported for directional boreholes with standalone executable software where users may import their 3D database files. In addition, not only attribute files but also optional files can be entered into the program.

1.2 Geographic Location and Geology of the Study Areas

In this study, two- and three-dimensional anomaly mapping through U-stats is applied to two separate mineralizations located in the Eastern Pontide belt in NE Türkiye. This E-W-extending belt is characterized by widespread Mesozoic-Cenozoic magmatic activity that developed in response to subduction of the Northern Neotethys basin that was located between the Pontide Fragment in the north and the Tauride-Anatolide Block in the south.

The northward subduction of the Northern Neotethys ocean resulted in development of a magmatic arc in the Late Cretaceous (Robinson et al., 1995, Okay and Şahintürk, 1997, Karsli et al., 2010, and Kandemir et al., 2019). This was followed in the middle Eocene by a subsequent episode of collisional magmatism (Topuz et al., 2005, Kandemir et al., 2019).

Igneous rocks that formed during these two distinct periods host a large number of magmatic-hydrothermal deposits including volcanic-hosted massive sulfide (VHMS), porphyry, epithermal, and skarn/carbonate-replacement type deposits (Yigit, 2009, Kuşcu et al., 2019, and Rabayrol et al., 2023). In particular, the sector of the magmatic belt that remains between İspir (Erzurum) in the southwest and Artvin in the northeast contains most of the economic mineral systems, which collectively comprise the Yusufeli camp and the Hod Gold Corridor. These mineralizations are regarded as some of the most attractive metallic ore systems in Türkiye and include regionally important deposits/prospects such as Hod Maden, Berta, Taç, Çorak, Salınbaş, Ardala, and Hızarlıyayla.

The Taç gold deposit is one of the few important mineralizations discovered in the Eastern Pontides. Taç is located about 7 km southwest of the Yusufeli district of Artvin, and is one of the main gold targets of the Hod Gold Corridor. Taç mineralization is located at the most southwestern sector of this corridor, while Corak, Ardala, Berta, and Salınbaş Au mineralizations are located in the northeast towards Yusufeli (Figure 3.1).

Taç comprises a vein-type epithermal-style gold system exposed within a NE-SW-trending valley that has been incised by the waters of the Çoruh River (Figure 3.2).

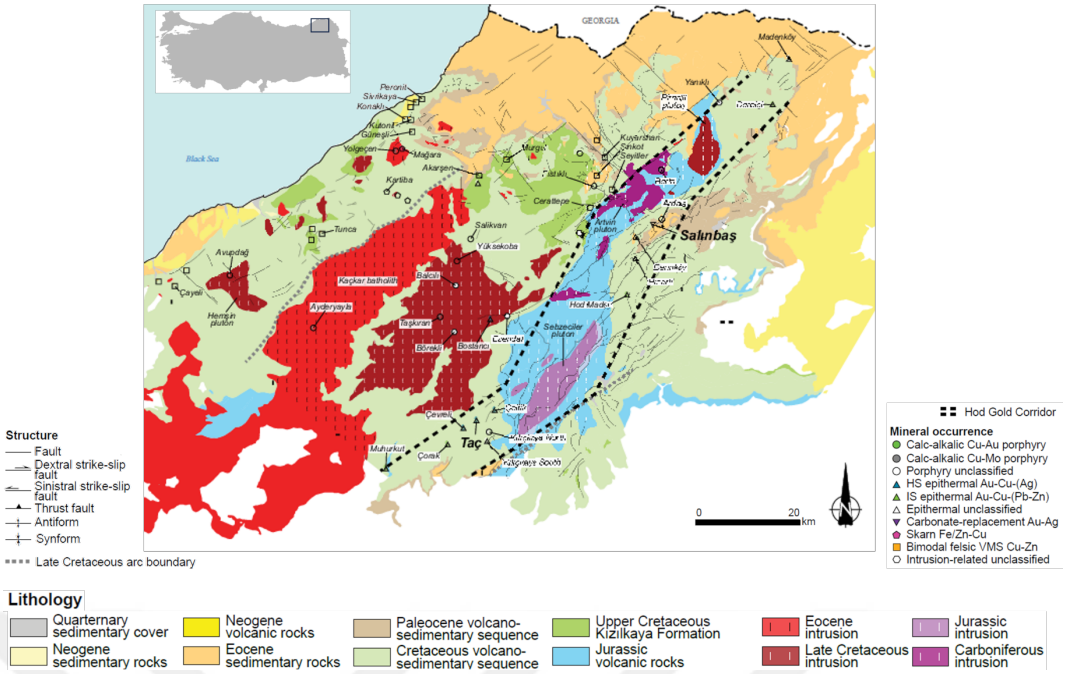


Figure 1.1: Geologic map of the study area showing the distribution of magmatic hydrothermal mineral occurrences, lithologies, and the Hod gold corridor (bold dashed line). Modified from Rabayrol et al., 2023

Mineralized veins are hosted in altered volcanic rocks that are andesitic to dacitic in composition (Figure 1.2). At Taç, most mineralization occurs in two topographically prominent domains to the north of the Çoruh River, namely the Karşıbayır Tepe and Kızıl Tepe (Figure 3.2). Within these two domains a preliminary resource of 0.95 Moz Au was delineated with average grades of 1.24 g/t Au and 0.12% Cu (Barnett et al., 2011).

Mapping at the site by geologists of Teck Resources and Santral Madencilik indicated that the volcanic sequence is bounded to the north and south by two sub-parallel normal faults that also run parallel to the main course of the river (Figure 3.12a). Within this structural corridor, volcanic stratigraphy is dominated by volcaniclastic rocks (agglomerate and tuff), and massive lavas locally cut by sub-volcanic intrusions (Figure 1.2). U-Pb zircon dating of this sequence at Taç and Corak indicated a Late Cretaceous timing (86 to 82 Ma) for volcanic activity at the district (Rabayrol et al., 2023).

In 2022, TUBITAK 1001 Project entitled *"Implicit Modeling of Hydrothermal Min-*

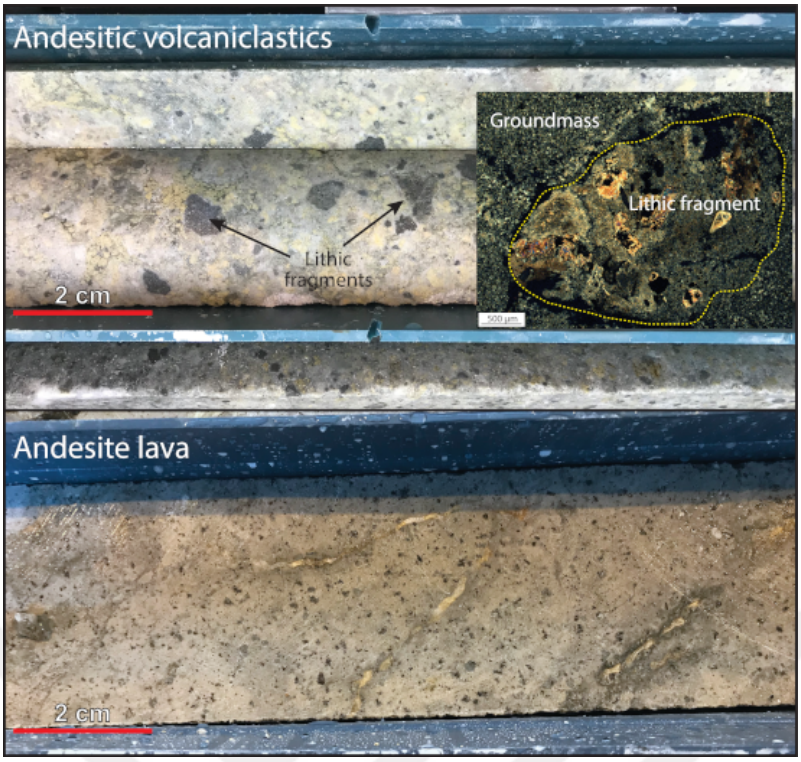


Figure 1.2: Google Earth image of the Taç field and gold mineralization view in the field, (b) General view of the mineralization (photo faces north-northwest)

eral Deposits with Indicator Kriging Based Support Vector Machines: Case Study of Taç Altın and Kurşunkaya Iron Deposits" was completed out by Ertunç et al., 2018. A site visit was carried out during February 2020 with the aim of sampling and quick logging of drill cores representing Taç mineralization. A total of 133 core samples were collected from five drill holes. Logging was carried out and detailed sampling was carried out especially from the intervals showing different types of alteration, mineralization, host rock, and textural features for the purpose of mineralogical-petrographic characterization, including comprehensive X-ray diffraction and thin section analysis. During the studies, the digital database obtained from Santral Madencilik and containing data for Au, Cu, Pb, Zn on the basis of meters of each are utilized.

Drill core observation and petrographic work indicated that all volcanic units at Taç show some degree of alteration. Three main alteration styles were identified including widespread argillic alteration (Figure 1.2), and more vein proximal silicification and

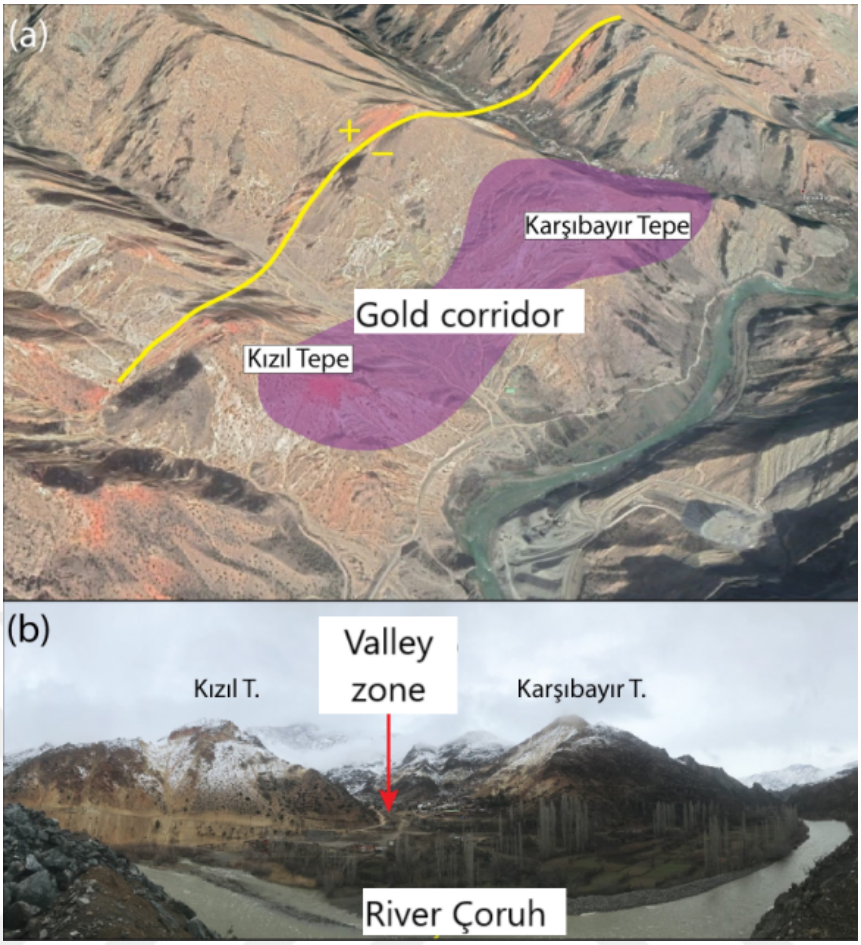


Figure 1.3: Google Earth image of the Taç field and gold mineralization view in the field, (b) General view of the mineralization (photo faces north-northwest)

carbonatization. Propylitic alteration (chlorite-epidote-carbonate-pyrite) envelopes these alteration styles and is not directly associated with mineralization.

Argillic alteration dominates the Taç corridor and has developed in the entire volcanic stratigraphy surrounding the mineralized veins. In argillized rocks, primary textures are generally preserved. However, feldspars and ferromagnesian phases (possibly amphibole and biotite) have been transformed into clay and white mica. XRD analyses revealed kaolinite and illite as the main clay mineral phases, whereas at depth sericite (muscovite) appears and dominates over illite. Minor chlorite, smectite, and rutile were also identified in argillized rocks.

All veins at Taç are closely associated with narrow (<20 cm) zones of silicification (Figure 1.4). In silicified rocks, all phenocryst and groundmass phases have been

altered into silica, mainly to microcystalline quartz. More coarse-grained quartz varieties were also detected adjacent to massive veins and breccia veins.

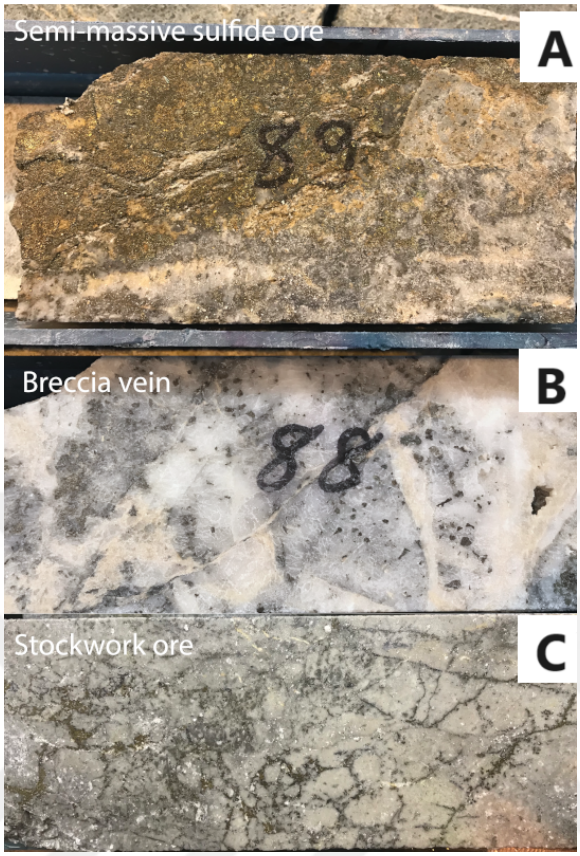


Figure 1.4: Representative drill core photos of Taç Au mineralization. A: Semi-massive sulfide ore containing high grade Au (approximately 900 g/t) in pyrite-chalcopyrite mineralization. B: Characteristic siliceous breccia vein containing >5 g/t Au. C: Pyritic stockwork breccia vein. All cores are in HQ diameter.

Carbonatization developed at relatively later stages within vein and breccia zones. Carbonate-rich, light-colored haloes around mineralized veins are typically narrow (<5 cm) and comprise coarse, rhombohedral dolomite crystals.

Taç is dominated by a series of narrow quartz-rich stockwork sulfide veinlets and also by breccia veins (Figure 1.5 and Figure 1.4). Stockwork veins range in thickness from 1 mm up to 3 cm. Pyrite and chalcopyrite accompany quartz in these veins, which are associated with low gold grades of less than 0.5 g/t Au (Figure 1.4 and Figure 1.5).

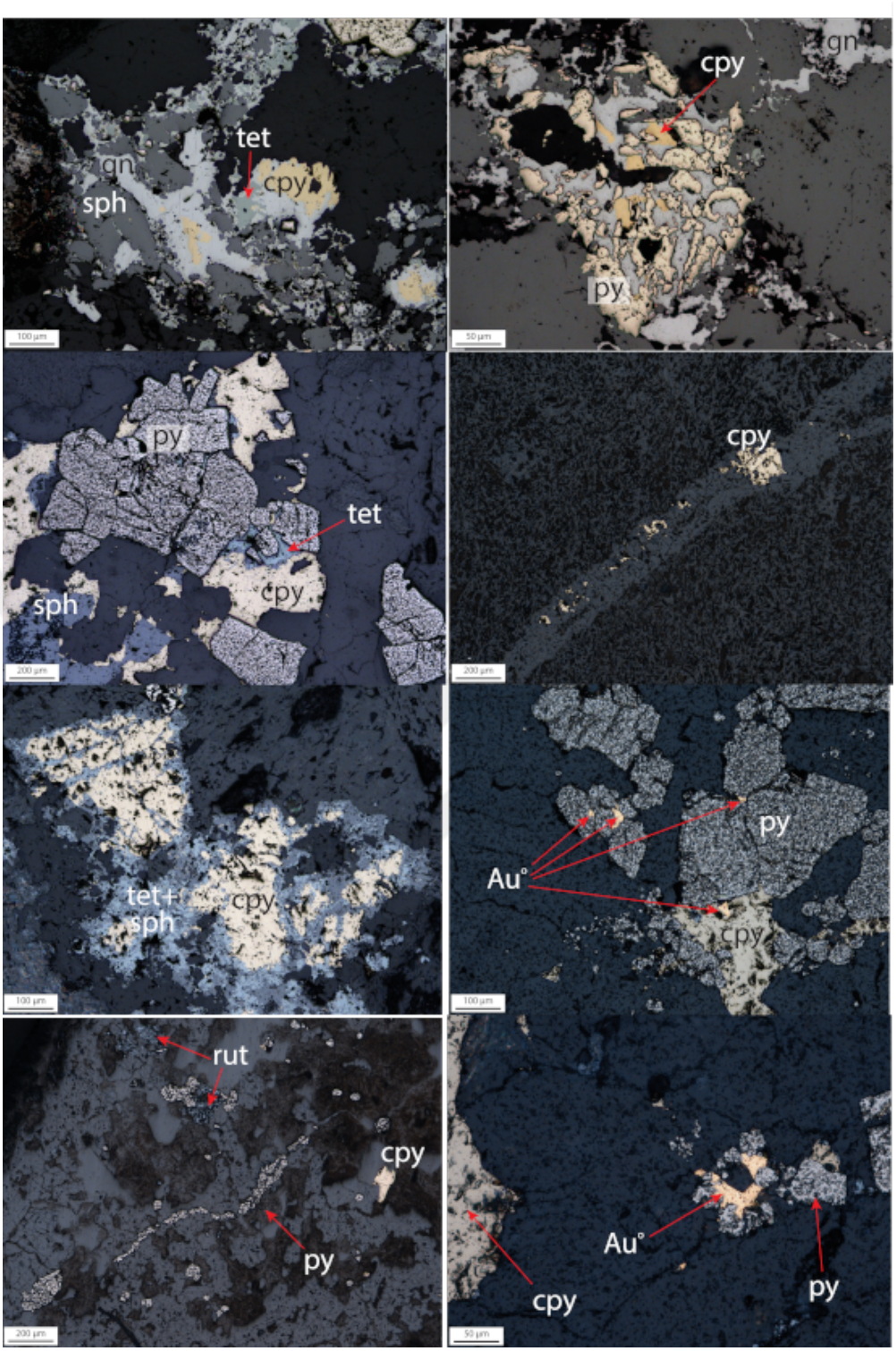


Figure 1.5: Microphotographs of Cu Au mineralized samples from Taç. All photographs are reflected plane-polarized light images. Abbreviations: cpy=chalcopyrite, gn= galena, py=pyrite, rut=rutile, sph=sphalerite, and tet=tetrahedrite

Crustiform banded veins cross-cut stockwork quartz-sulfide veinlets (A-C Figure 1.6). These are thicker and are characterized by well-developed, euhedral quartz that are developed in symmetrically developed bands on the vein margins (B-C Figure 1.6). Pyrite and chalcopyrite appear as central vein fill in these veins, whereas carbonate occurs as a late stage vug fill.

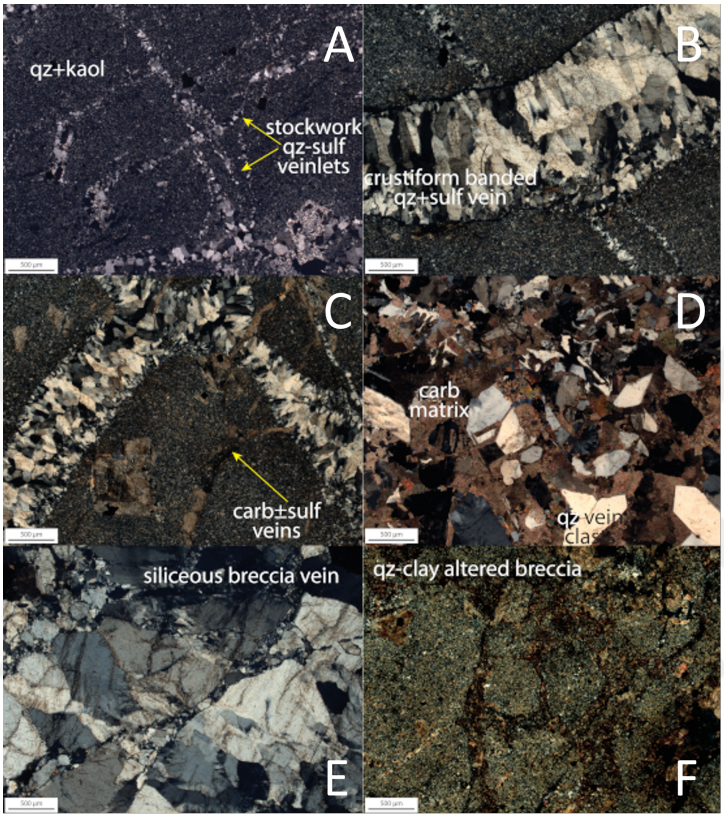


Figure 1.6: Microphotographs of common ore textures from Taç. A: Quartz-sulfide stockwork veinlet in argillic altered andesite lava. B-C: Crustiform banded quartz-sulfide veins cross-cutting stockwork veinlets. D: Breccia vein consisting of mineralized siliceous vein clasts surronded by carbonate matrix. E: Intensely deformed siliceous breccia vein. F: Brecciated and argillic altered andesite. All photographs are transmitted, cross-polarized light images. Abbreviations: carb=carbonate, kaol=kaolinite, qz:Quartz, sulf=Sulfide

High gold and copper grades as well as significant Pb and Zn enrichment occurs in association with breccia veins (D-F Figure 1.6 and Figure 1.4). These veins are dominated by early stage quartz-pyrite-chalcopyrite and carbonate developed in the later

stages of vein/breccia development. In vein breccias gold grades are generally between 0.2 and 2 g/t Au. However, in zones of structural deformation, these veins appear to be intensely deformed (as indicated by cataclastic and sheared quartz). As a consequence, breccia veins were re-opened and paragenetically late sulfide phases as well as some carbonate precipitated. In deformed breccia veins, pyrite and chalcopyrite were overprinted by sphalerite, galena, and carbonate as well as by minor tetrahedrite group minerals. In such veins, native gold was also detected and as such gold grades typically reach up to 20 g/t Au (Figure **??**), with a maximum gold assay of 896 g/t from a zone of semi-massive sulfide-rich breccia vein (A in Figure **??**).

The Salınbaş gold prospect is located about 20 km east of Artvin, within a district that shows distinct mineralization styles. The nearby Ardala porphyry prospect is located only about 2.5 km to the northeast and is centered around a series of porphyritic intrusions (Figure 1.7).

The Salınbaş mineralization developed along the unconformable contact between Late Cretaceous (100 Ma) Ziyarettepe Formation and Late Paleocene (56 Ma) Kızılcık Formation (Fig). The former comprises fossiliferous limestone units, whereas the latter is represented by a sedimentary sequence of intercalating conglomerate, limestone, siltstone, and mudstone/shale (Groves et al., 2017).

The Salinbas orebody is dipping ENE and has a thickness varying between 5 and 10 m (Groves et al., 2017). It has been interpreted as a carbonate-replacement type mineralization, in which sulfide-rich breccia zones with semi-massive to massive sulfide mineralization is present (Groves et al., 2017). The Salınbaş project has estimated resources of about 8.4 Mt at 2.21 g/t Au, 10.2 g/t Ag (0.65 Moz Au; Resources, last visited on October 2023)

1.3 Previous Studies

In geochemical anomaly detection, it has traditionally been established that the mean and median values of lognormal distributions are used to determine sediment and soil background values (Rose et al., 1979; Wang et al., 1999). Until the end of the 19th century, the median of the lognormal distribution was suggested by Levinson, 1974

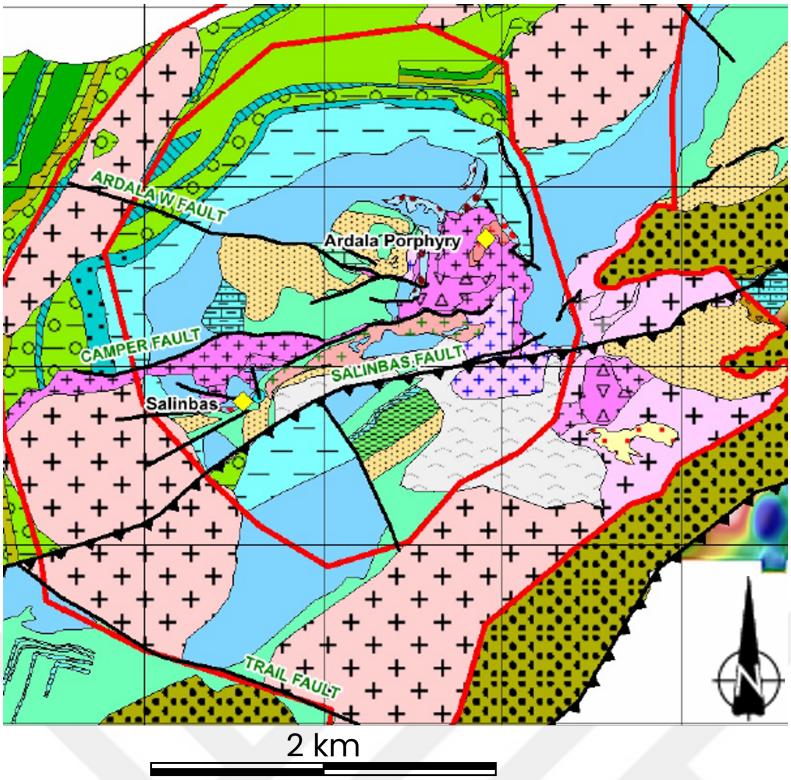


Figure 1.7: Map of the Ardala-Salınbaş area showing the distribution of plagioclase-acicular-hornblende magnetite bearing porphyritic intrusions (light pink with large crosses) in a rough circular pattern around the central Ardala Porphyry swarm (magenta). The red lines show a possible circular pattern to the plagioclase-acicular-hornblende magnetite bearing porphyritic intrusions distribution with a 5km diameter. The topographically higher ground to the SE, has preserved the flanking Avicular Formation (khaki spotty rock), which possibly erupted from the core of this circular intrusive complex. Modified from Groves et al., 2017

as the background. The median + 2MAD (Median absolute deviation) approach of exploratory data analysis has been extensively utilized to differentiate geochemical anomalies from the background (Asadi et al., 2014; Carranza, 2008; Reimann and Garrett, 2005).

Later studies suggested that fractal analysis is a more dependable method than median + 2MAD and mean + 2SD to determine stream sediment background levels (Afzal et al., 2016, Carranza, 2010, Arias et al., 2012, Gonçalves et al., 2001, Hao et al., 2014, Li et al., 2003, Li et al., 2003, Luz et al., 2014). Carranza, 2010 has established

that in the surveying of stream sediment anomalies, the C–A Fractal Method -which is formulated and proposed by and Cheng et al., 1994- was more effective than the Median + 2MAD and Mean + 2 σ approaches of determining the threshold values. Reimann et al., 2005 presented comprehensive comparison between background and threshold determination methods.

In Türkiye, published work on detection of geochemical anomalies around metallic ore deposits are rare. These studies generally followed approaches similar to that was explained above such that they attempted to identify geochemical signatures of mineralization through surface geochemical data (e.g., soil, rock, and/or stream sediment sampling data). These studies almost mainly focused on gold systems and used lognormal distribution for distinguishing anomalies from background values. Yilmaz, 2003 studied both in local (stream sediment and soil) and regional scale (BLEG) geochemical sampling for discovering precious and base metal occurrences in Türkiye in which the median of lognormal distribution is assumed as the background value. Yilmaz et al., 2015 also presented background and anomaly detection in Au-Ag-As mineralization located at Western Türkiye. The concentration–area (C–A) fractal model is applied in order to define thresholds. In Yilmaz et al., 2019, the examination of geochemical assay results through multifractal analyses uncovered gold geochemical anomalies connected to gold mineralization. Moreover, a singularity mapping technique was employed to amplify the single element geochemical signatures of BLEG sand stream sediment data.

1.4 Structure of the Thesis

This thesis consists of six chapters in total. The contents of these 6 chapters are listed as follows:

- Chapter 1 (p. 1) covers introduction, literature review, and purpose and scope of the thesis.
- Chapter 2 (p. 15) is dedicated to the methodology of U-Statistics.
- Chapter 3 (p. 17), Chapter 4 (p. 27), and Chapter 5 (p. 37) are related to the

Matlab Graphical User Interface (GUI) of U-Statistics. Demo, 2D, and 3D interfaces are given in detail, respectively.

- Chapter 6 (p. 49) are dedicated to the 3D interface with Taç and Salınbaş case studies
- Chapter 7 (p. 69) gives the conclusions and future works.

CHAPTER 2

METHODOLOGY

U-Statistics utilizes similar approach to a moving average where the window size shifts at each point. Subsequently, U-statistics for a point are determined by the points in its neighborhood. This neighborhood definition is exactly the same as the search neighborhood in kriging, the geostatistical estimation method. To begin with, vicinity criterion inside the search neighbourhood is set. This criterion depends on the distances between points inside neighbourhood and target location. It is described in the Equation 2.1 (**Ghannadpour2016**; Cheng, 1999; Cheng et al., 1996).

$$\mu_{\kappa(x_i,r)}\left(x_j\right) = 1 - \frac{d\left(x_i, x_j\right)}{r} \tag{2.1}$$

where $\kappa\left(x_i, r\right)$ represents the search neighbourhood, x_j: samples inside search neighbourhood, x_i: target location, $d\left(x_i, x_j\right)$: distance from sample location x_j to target location x_i, and r is the major axis of search neighbourhood.

Properties of $\mu_{\kappa(x_i,r)}\left(x_j\right)$ as follows:

$$0 \leq \mu_{\kappa(\alpha_i,r)} \leq 1$$

and

$$\mu_{\kappa(x_i,r)}\left(x_j\right) = \begin{cases} 1 & \text{if } x_j = x_i, \\ 0 & \text{if } x_j \notin \kappa\left(x_i, r\right) \end{cases}$$

The weights attached to the samples inside the neighbourhood (w_j) is basically the arithmetic mean of the vicinity measures described in Equation 2.1. Its formula is given in Equation 2.2.

$$w_j = \frac{\mu_{\kappa(x_i,d)}(x_j)}{\sum_{j=1}^{n} \mu_{\kappa(x_i,d)}(x_j)} \tag{2.2}$$

where $0 \leq w_j \leq 1$, $\sum_{j=1}^{n} w_j = 1$, and n is the sample count inside the search neighbourhood.

Estimation value at the target location (Z_i^*) is then calculated as in Equation 2.3.

$$Z^*(x_i) = \sum_{j=1}^{n} w_j Z(x_j) \tag{2.3}$$

where w_j: weight of sample at location x_j, $Z(x_j)$: attribute value at location x_j.

In the next step, square root of squared sum of the weights are calculated (Equation 2.4). This dispersion measure is then used in standardization when defining U-Stats given in Equation 2.5.

$$S_i = \sum_{j=1}^{n} w_j^2 \tag{2.4}$$

U-Stats of target location (U^*) at location x_i is linear combination of $Z(x_j)$ and defined as in Equation 2.5:

$$U^* = \frac{Z^*(x_i) - \mu}{\sum_{j=1}^{n} w_j^2 \, \sigma} \tag{2.5}$$

Here, S_i: dispersion measure, μ: mean, σ is the standard deviation of all raw data.

CHAPTER 3

U-STATS GUI: DEMO, CHENG ET AL. 1996

First option of U-Stats GUI is dedicated to the journal article Cheng et al., 1996. In this option, reproduced case study of the paper is presented and covered in detail. Additionally, user may modify U-Stats input parameters and study the effects of the parameters on the results. QR code in "Demo, Quiming Cheng et al. 1996" (Demo, in short) selection window (Figure 3.1) is directing user to the link of the article URL.

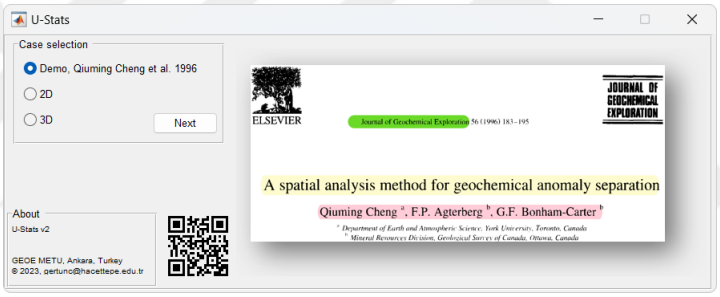


Figure 3.1: U-Stats GUI main window, Demo selection

In this publication, the authors introduced the U-Stats in a random space assumed to have 2500 samples at regular intervals in a square area with a side of 50 km. There are two anomaly zones, named A1 and A2, cover 78 and 125 km^2, respectively, and the total anomaly area corresponds to 8.1% of the total area. The background area is determined as 2297 km^2. Anomaly zones and background area attributes have a normal distribution. Standard deviation and mean values (σ, μ) for the anomaly zones A1 and A2 are (15, 25) and (10, 30), respectively. Background area's standard deviation and mean value has set to 20 and 10, respectively.

In this Demo case of the thesis study, same distribution scheme for all zones presented in the paper are simulated, coded, and merged into GUI. Also, all calculations have

been made in advance and the results have been saved beforehand. At the start of this option, original base map image captured from paper (Figure 3.2 (right hand side)) and reproduction of the sample zones (Figure 3.2 (left hand side)) is on display by default.

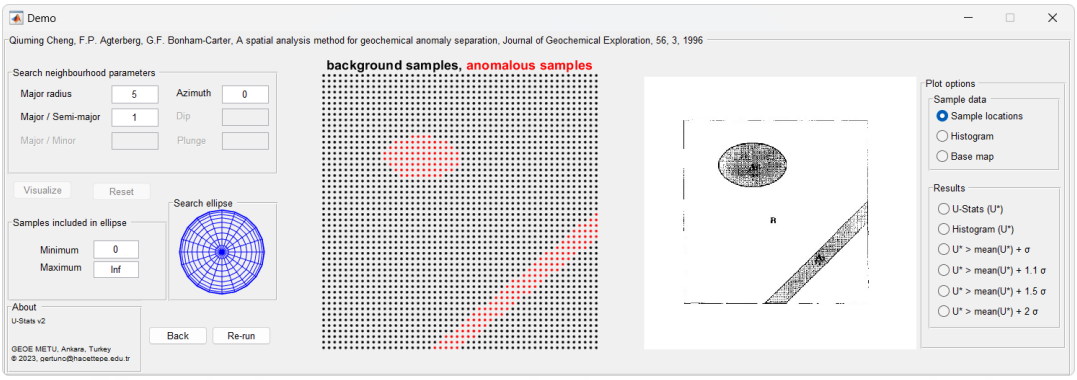


Figure 3.2: U-Stats GUI Demo: Main window

U-Stats GUI Demo main window has 4 panels (3 calculation and an informative) and 2 plot areas. The "Plot options" panel consists of two sub-panels. These are "Sample data" and "Results", respectively. As the names suggest, "Sample data" is related to the data to be used in calculations. First selection in "Sample data" (Figure 3.2) shows the red and black binary map of the background and anomalous samples. Second selection for "Sample data" is the histogram which is presented in Figure 3.3. "Results" panel is related to the results of U-Stats calculations which is covered in detail at Section 3.2.

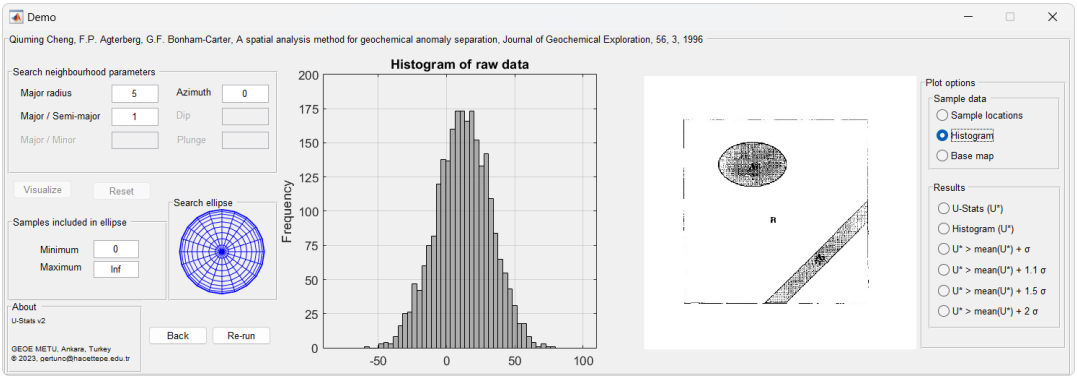


Figure 3.3: U-Stats GUI Demo: Histogram of raw data

In addition to the original publication, thematic visualization of sample attribute val-

ues is presented in the U-Stats GUI Demo (Figure 3.4). This selection is included to show that different anomaly regions are difficult to distinguish just by looking at the base map.

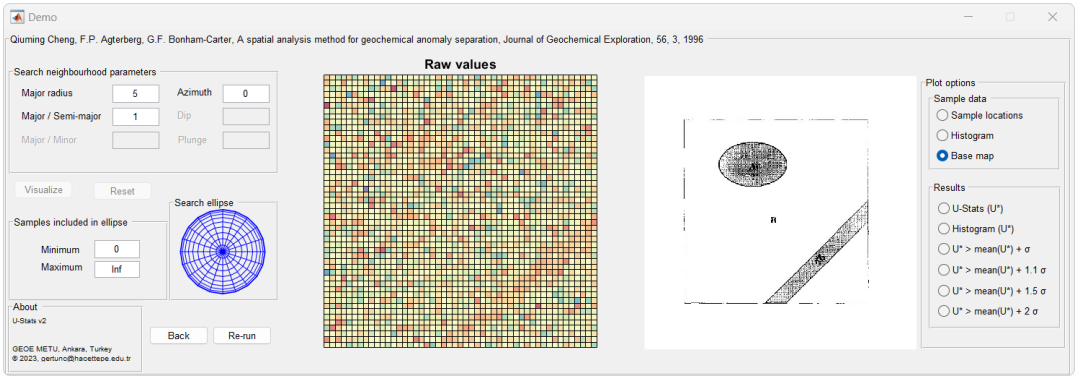


Figure 3.4: U-Stats GUI Demo: Base map

Other two panels, "Search neighbourhood parameters" and "Samples included in search ellipse" is described in the following section 3.1 Sample Selection Strategy.

3.1 Sample Selection Strategy

In the U-Stats GUI, the sample selection strategy is exactly same as in geostatistical estimation and simulation. In this strategy, an ellipse or ellipsoid (depending on the case whether it is 2D or 3D) is defined, which visits all block centeroids at target location sequentially. For each block, calculations are made with respected to the samples which are falling into the geometry of ellipse or ellipsoid. The samples to be used in the calculations is selected according to the size and orientation of the ellipse or ellipsoid located in the center of the block. Also, the number of samples to be used in calculations can be limited by the minimum and maximum number provided by the user. If no instances fall within the defined geometry, it is not possible to obtain a solution for that particular block. In Figure 3.5, schematic representation of 2D ellipse and 3D ellipsoid is presented. In 2D, in order to define ellipse, two axis are required. In the context of geostatistics and U-Stats calculations these are called the "Major" and "Semi-Major" radius. There is only one angle defined for the orientation which is called "Azimuth". It is defined as the clock-wise horizontal angle from the North. In

3D, one additional radius which is called "Minor" axis is defined. Furthermore, two vertical axis angles are needed to define orientation based on the X-axis and Z-axis that are called "Plunge" and "Dip", respectively.

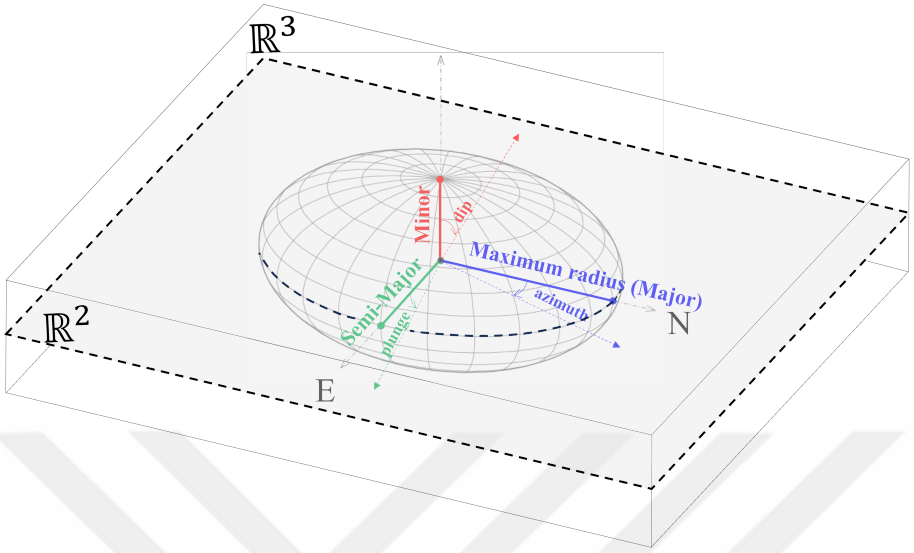


Figure 3.5: Geometric and angular parameters of ellipse and ellipsoid

Figure 3.6 visualizes an example of a 3D sample search strategy with the maximum number of samples set to "12". In the figure, the twelve sample points closest to the block center are colored in green and samples that will not be used in calculations are colored in red.

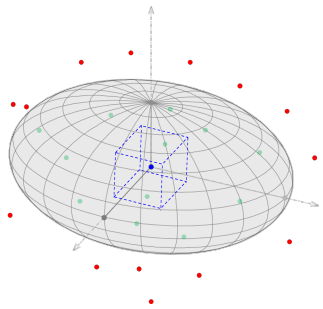


Figure 3.6: Samples around in ellipsoid (included: green dots, excluded: red dots)

"Search neighbourhood parameters" panel (Figure 3.2, 3.3, and 3.4) is related to the geometric aspects of the ellipse. Major radius, as the name implies, is the longest axis. Major/Semi-major ratio is for the calculation for the second axis of the ellipse. Major/Minor ratio is greyed out because U-Stats Demo GUI is in 2D space. "Azimuth"

edit box is for the orientation of the ellipse. "Dip" and "Plunge" edit boxes are related to 3D aspects and also greyed out. The "Minimum" and "Maximum" sample size in ellipse defines the minimum and maximum number of samples to be included in the ellipse, respectively. If there are more samples than the maximum sample size in the ellipse, the algorithm selects the closest samples according to their euclidean distances from the ellipsoid center with the "nearest neighbour" routine. "Inf" notation in the "Maximum" edit box defines infinite number of samples.

In the U-Stats GUI Demo case study, major radius is set to 5 m with isotropic search ellipse. The isotropic case can simply be defined as not varying according to the direction. Hence, the isotropic search ellipse is circle. The anisotropic cases (different characteristics in varying directions) are covered in Section 3.3.1 and 3.3.2.

3.2 Results

There are six plot options in Results panel under "Plot options". When any of the plot options selected, the map is displayed on the left hand side plot area. First plot option is U-Stats (U^*) (Figure 3.7). The color palette (RdBu: Red Blue) of the heat map is adapted from RColorBrewer (Neuwirth, 2022) from the R software package (R Core Team, 2023). Blue and red colors are representing low and high U^* values, respectively.

From Figure 3.7, it can be seen that U^* with isotropic search set up is in fair agreement with the ground truth.

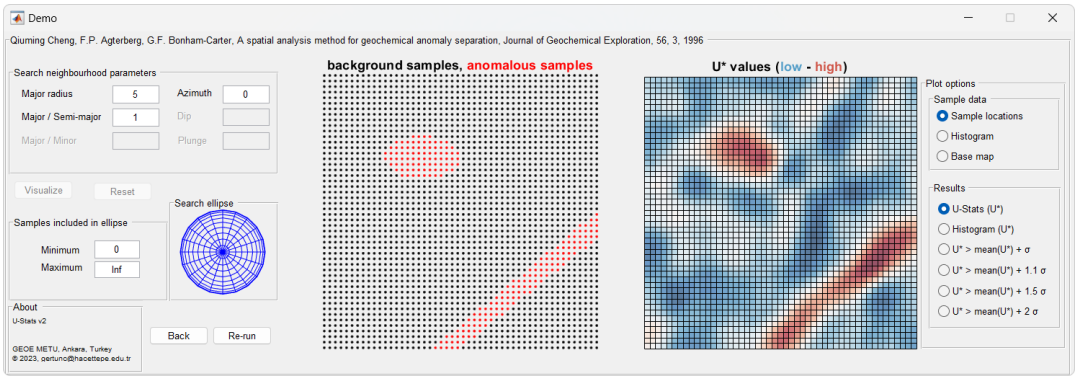


Figure 3.7: U-Stats (U^*) values

Second results plot option (Figure 3.8) is histogram of (U^*). As the main purpose of the U^* methodology is to distinguish anomalous samples from background values, in histogram plot it is expected to have multi-modal distribution. When Figure 3.8 is inspected, this bimodal distribution can clearly be seen.

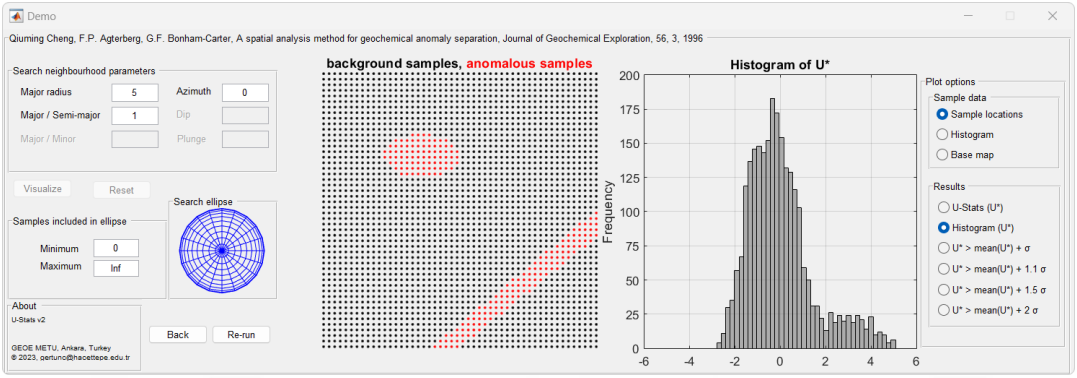


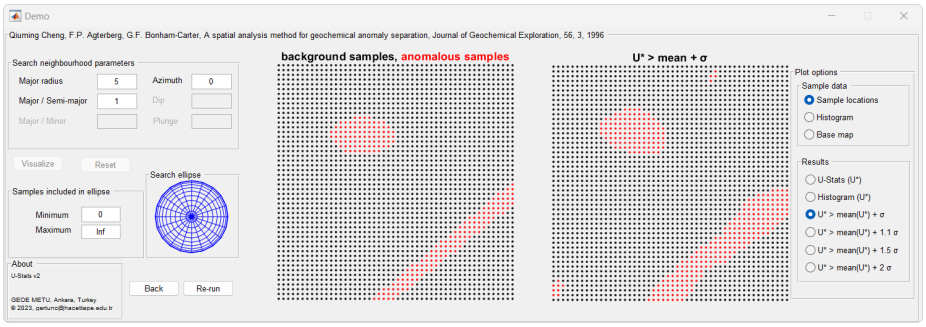
Figure 3.8: Histogram of U^*

In Figure 3.9, rest of the results plots are presented. In order to clarify anomalous zones, algorithm transforms U-Stats (U^*) values into binary variables based on the thresholds mean(U^*) + σ (Figure 3.9a), mean(U^*) + 1.1 σ (Figure 3.9b), mean(U^*) + 1.5 σ (Figure 3.9c), and mean(U^*) + 2 σ (Figure 3.9d). Multipliers of the standard deviation σ can be considered as confidence levels, just like the confidence interval in statistics. Target locations having U^* greater than threshold labeled as "anomalous" and rest of the locations ($U^* \leq$ mean(U^*) + $\times$ σ) are "background". Here, $\times$ is multipliers of the standard deviation.

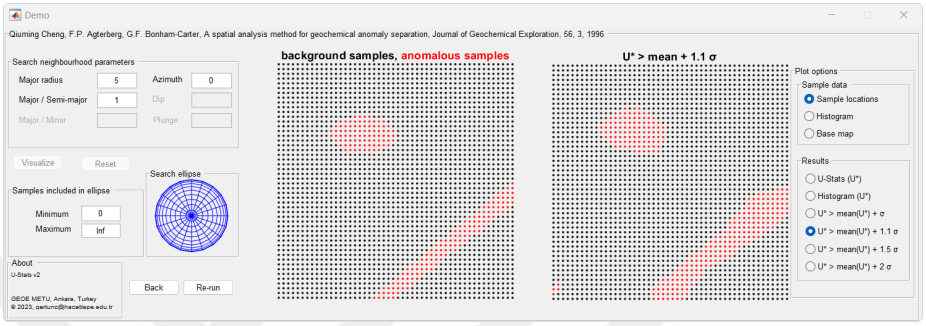
3.3 Re-run

Users may re-run the current demo data with customized parameters by clicking the "Re-run" button. In default re-run setup, "Search neighbourhood parameters" and "Samples included in search ellipse" panels are enabled and "Results" under "Plot options" are greyed out until calculations are made (Figure 3.10).

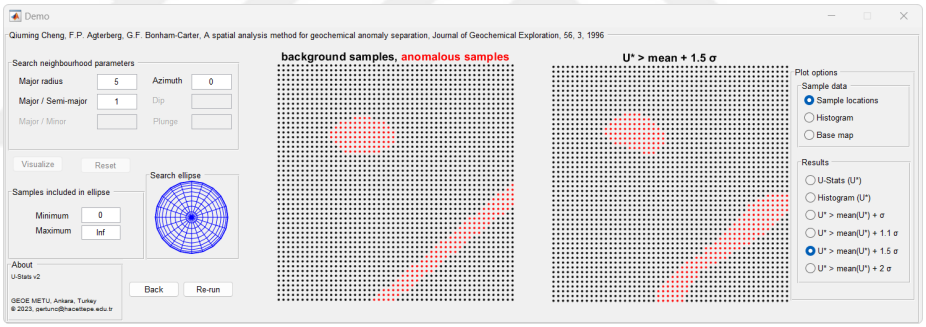
The anisotropy characteristics in the two anomaly zones in the U-Stats Demo GUI example are different from each other (Figure 3.2, 3.3, and 3.4). The anisotropy direction (major axis azimuth) in the A1 zone is 90°, the major axis is about 14 km,



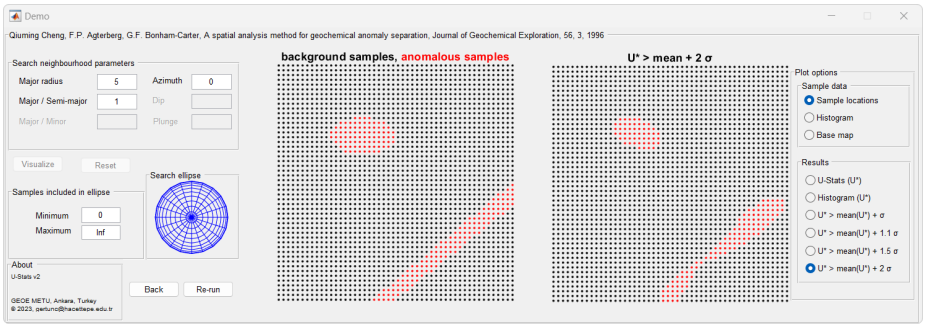
(a) mean(U^*) + σ



(b) mean(U^*) + 1.1 σ



(c) mean(U^*) + 1.5 σ



(d) mean(U^*) + 2 σ

Figure 3.9: Result plots

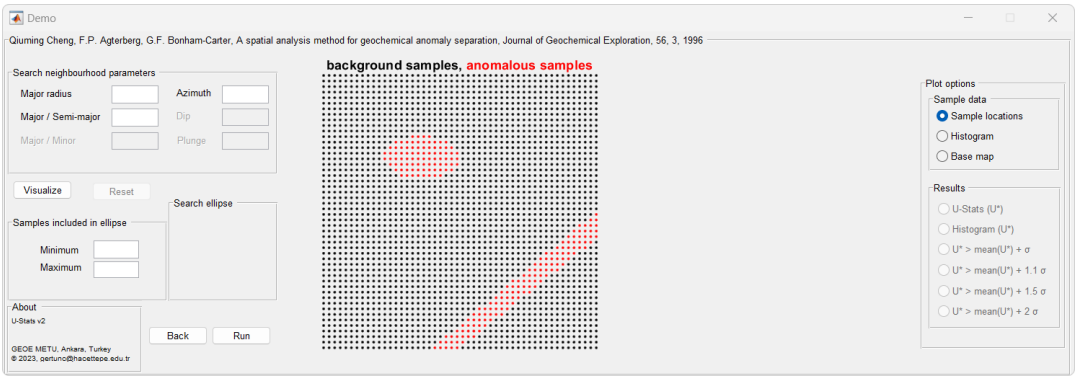
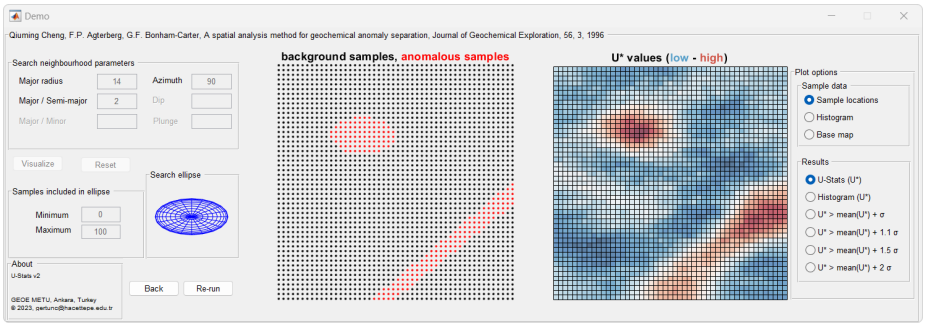


Figure 3.10: Re-run screen

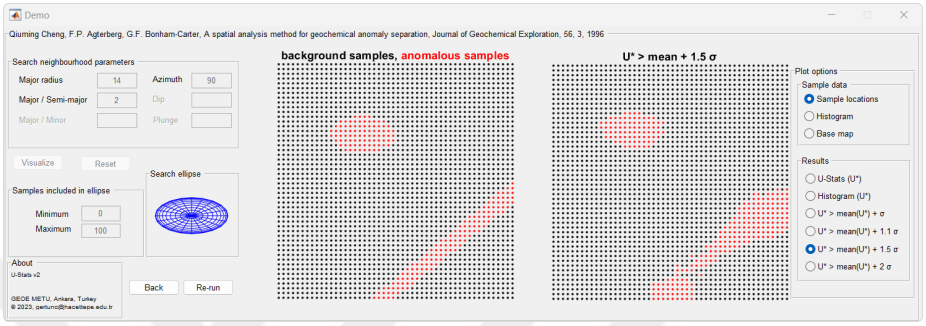
and the anisotropy ratio (Major/Semi-major) is 2. The anisotropy type of A2 zone can be described as zonal anisotropy. In zonal anisotropy, correlation is stronger in one direction than it is in the other directions. Here, continuity in the azimuth direction of approximately 50° is more dominant than in other directions. Since two anomalies cannot be determined with the same search neighbourhood parameters, re-runs were investigated in separate subsections, Section 3.3.1 and 3.3.2, respectively.

3.3.1 A1 anomaly zone

In this re-run, parameters compatible with the geometric continuity of the A1 anomaly zone (Major axis=14 km, Major/Semi-major=2, Azimuth=90°) were chosen. The number of samples included in the search ellipse is bounded between 0 and 100. Results of the re-run are given in Figure 3.11. Due to the search ellipsoid chosen in accordance with the geometry of the A1 anomaly zone, the U-Stats (U^*) values of the A1 anomaly zone (Figure 3.11a) seem to reflect the reality more clearly than the A2 anomaly zone. From the four binary threshold options, only mean(U^*) + 1.5 σ is chosen as a representative and given in Figure 3.11b. In this figure, it is seen that the geometric structure of the A1 anomaly zone is produced in accordance with ground truth. However, when the A2 anomaly zone is examined, it is seen that the results are not considered successful.



(a) re-run A1 anomaly U-Stats (U^*) values



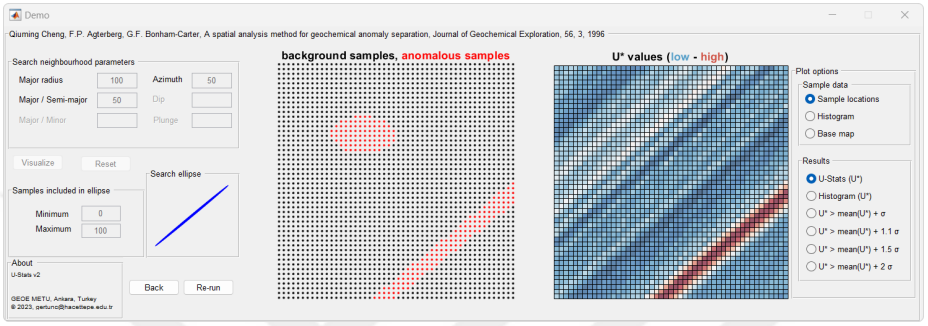
(b) re-run A1 anomaly, mean(U^*) + 1.5 σ

Figure 3.11: Result plots: A1 anomaly zone

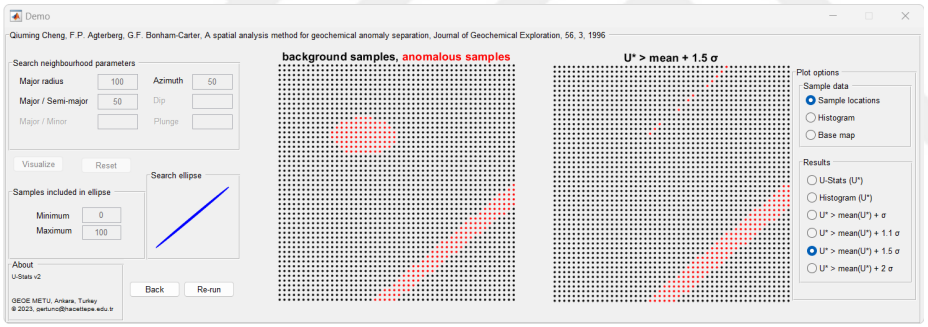
3.3.2 A2 anomaly zone

As mentioned above, A2 anomaly zone has zonal anisotropy characteristics. In order to reflect this structure, anisotropy ratio should be selected relatively high (in this case 50). Major axis and azimuth of the search ellipse is set to 100 km and 50°, respectively. Same sample count configuration as in the previous section is used (minimum=0, maximum=100).

Results of the re-run are given in Figure 3.12. It can be seen that the U-Stats (U^*) values (Figure 3.12a) in the A2 anomaly zone are significantly higher than in the A1 anomaly zone. Figure 3.12b represents the rerun results mean(U^*) + 1.5 σ binary map. While the results of the A2 anomaly zone are almost identical with the ground truth, the determination of the A1 anomaly zone could not be achieved due to the search ellipse geometry.



(a) re-run A2 anomaly U-Stats (U^*) values



(b) re-run A2 anomaly, mean(U^*) + 1.5 σ

Figure 3.12: Result plots: A2 anomaly zone

CHAPTER 4

U-STATS GUI: 2D

Two dimensional cases are available through the main U-Stats GUI options (Figure 4.1).

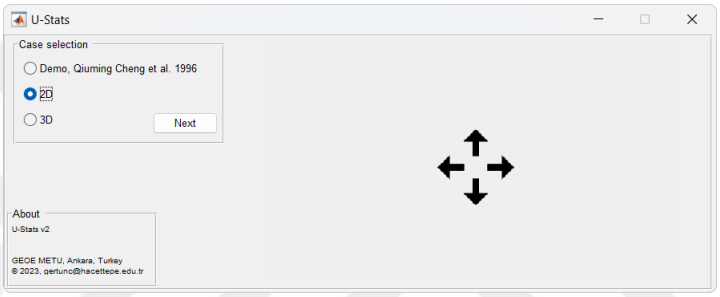


Figure 4.1: U-Stats GUI main window: 2D selection

In this chapter, U-Stats GUI: 2D is introduced with realistic epithermal Au field rock samples. Total number of rock samples are 198 and Au grades (in ppm) at each coordinate are stored in Microsoft® Excel® (*.xlsx) file. All steps from the data import to result export steps are given in detail at the corresponding subsections.

4.1 Data Import

First step of the U-Stats GUI: 2D is data import (Figure 4.2). In the context of U-Stats GUI, the folder that contains all files related to the project is called the "working directory". The program starts when the user selects this folder. There are three mandatory fields in this window to be matched. These are Northing (Y coordinate component), Easting (X coordinate component), and the Attribute (quality or feature regarded as a characteristics of random variable), respectively.

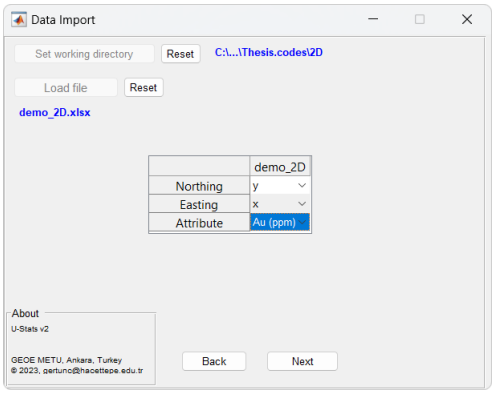
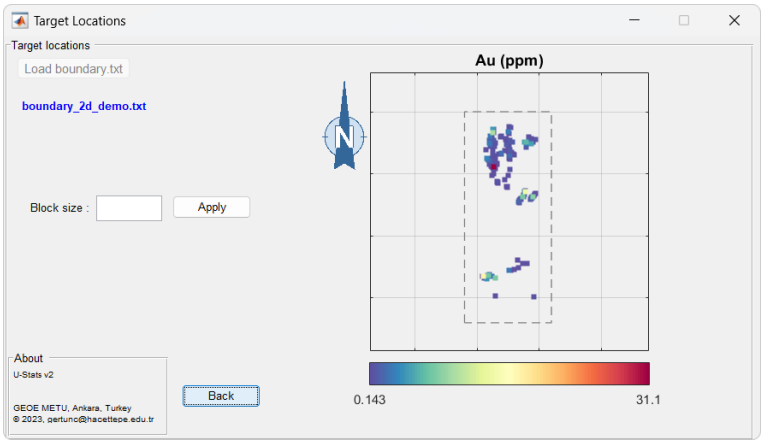


Figure 4.2: U-Stats GUI: 2D, data import

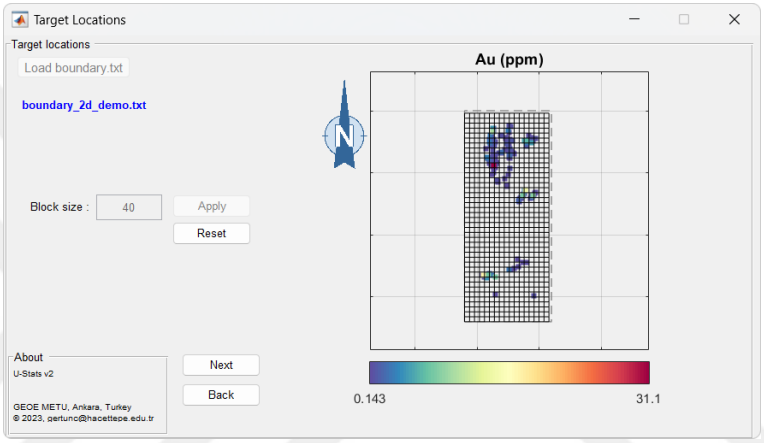
4.2 Target Locations

Target locations can be defined as the calculation space or grid. After the data is successfully imported, following step is to load the boundary. This boundary, which is in the ASCII format, defines the region where the U-Stats are calculated. In Target locations window, base map of sample locations are colored by the attribute with color palette. The color palette (RdYlBu: Red Yellow Blue) is adapted from RColorBrewer (Neuwirth, 2022) from the R software package (R Core Team, 2023). In this case study, loaded boundary representation in GUI is visualized in Figure 4.3a (Grey dashed line).

This version (v2) of U-Stats GUI: 2D supports blocks in square form. When the block size is given and applied by the user, grid of blocks are visualized on the screen (Figure 4.3b). The blocks automatically fill the bounded region starting from the westernmost and southernmost coordinates of the boundary file provided in the first phase. With the Next button, the run and results screen is accessed.



(a) Boundary region (Grey dashed line)



(b) Grid of blocks

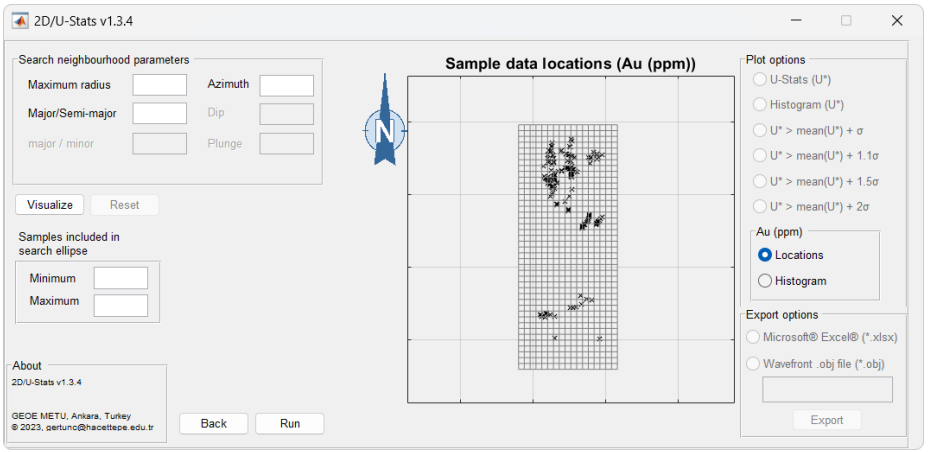
Figure 4.3: U-Stats GUI: 2D, target locations

4.3 Run and Results

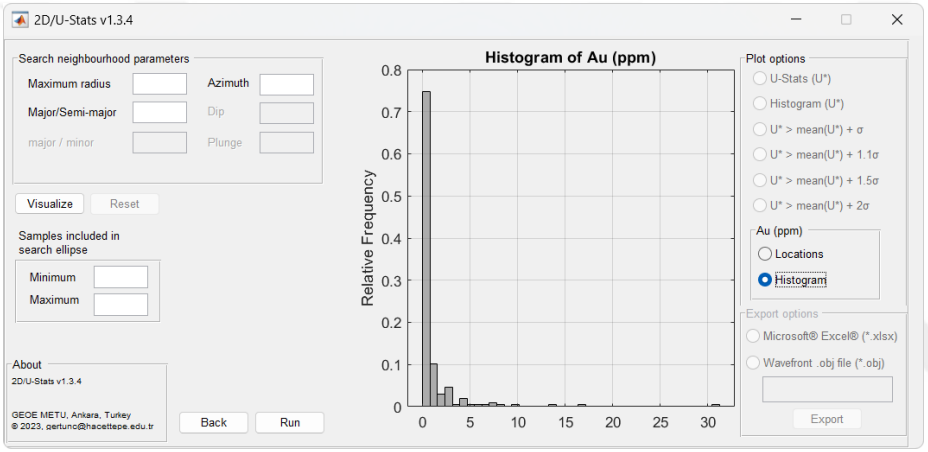
Run and Results screen in U-Stats GUI: 2D has four panels and one plot area. Two panels ("Search neighbourhood parameters" and "Samples included in search ellipse") are related to the run parameters of the U-Stats. Third panel is "Plot options" which is for sample data and results related plots. Finally, there is "Export options" panel. As the name suggests, this is for exporting results in Microsoft® Excel® (*.xlsx) and Wavefront .obj file format.

When this window is on display for the first time, on the plot area, location map of the sample data with target blocks is visualized automatically (Fig 4.4a). Second option

related to the samples is histogram plot (Fig 4.4b).



(a) Sample locations



(b) Histogram of sample data

Figure 4.4: U-Stats GUI: 2D, sample related plots

In Search neighbourhood parameters panel, user defines ellipse that is utilized for the sample selection in U-Stats calculation. Maximum radius, Major/Semi-major, and Major/Minor are related to the geometric aspects of ellipse. Azimuth, Dip, and Plunge parameters are related to the angular rotation of the ellipse. User interface, codes, and functions are completely adapted from U-Stats GUI: Demo (CHAPTER 3).

In U-Stats GUI: 2D, Major/minor ratio, Dip, and Plunge parameters are disabled and greyed out, since this window is designated for 2D solution space.

Once the search neighbourhood parameters and sample sizes are given by the user the program is ready for the run. The ellipse that will be used in the solution can be displayed by Visualize button. The red ellipse is drawn in 1:1 scale and located at the middle of the target blocks, as a representation of search ellipse (Figure 4.5).

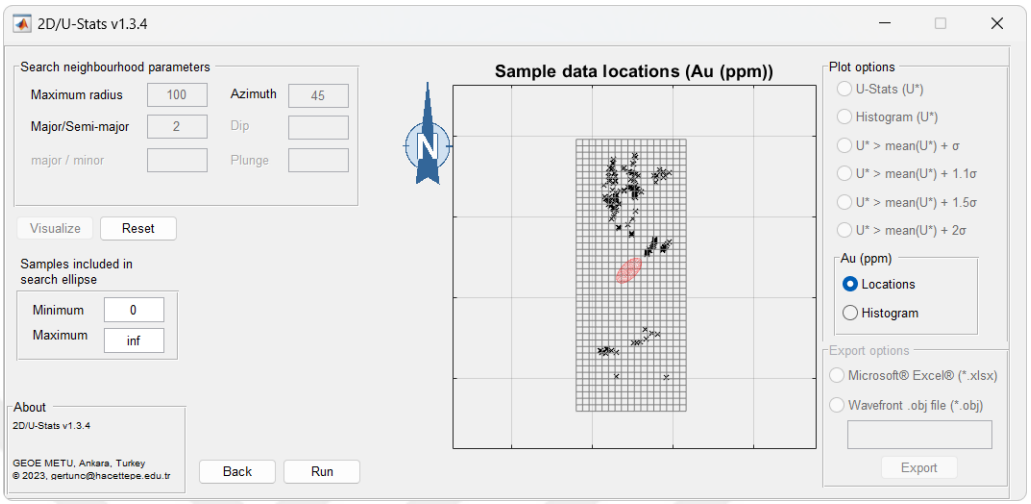
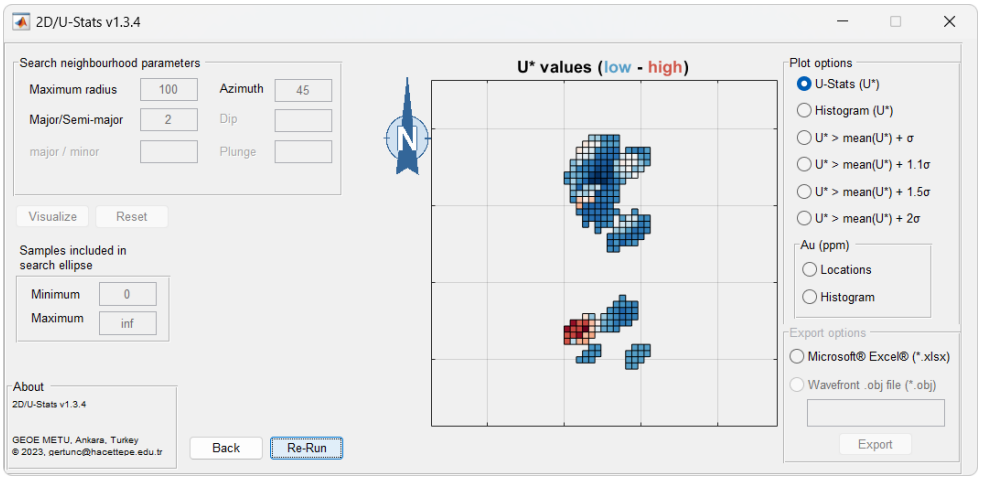


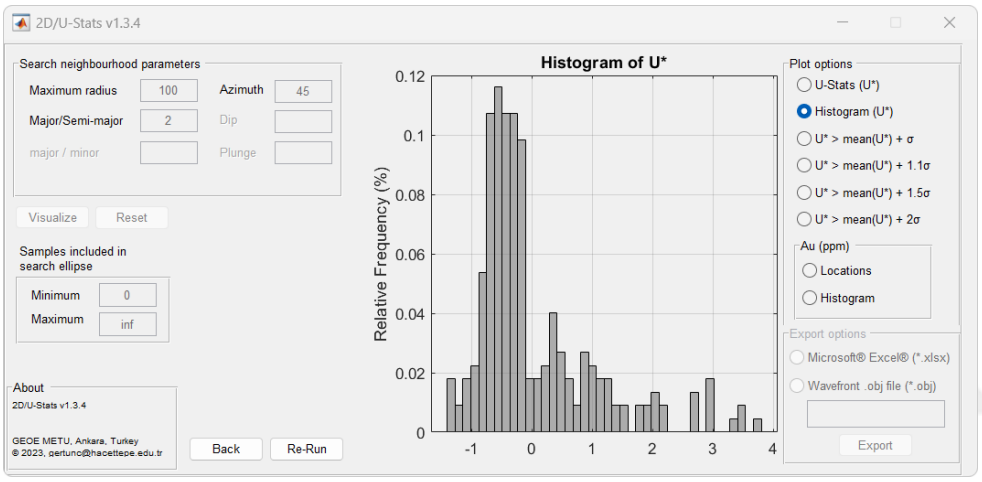
Figure 4.5: U-Stats GUI: 2D, search ellipse (in red)

U-Stats GUI: 2D utilizes same result plots configuration with U-Stats GUI: Demo which is mentioned in "3.2 Results".

From the histogram of the U-Stats results 4.6b, it can be clearly seen that it is in the form of multi-modal distribution. This concludes there are two different sub-population (background and anomaly) exists.



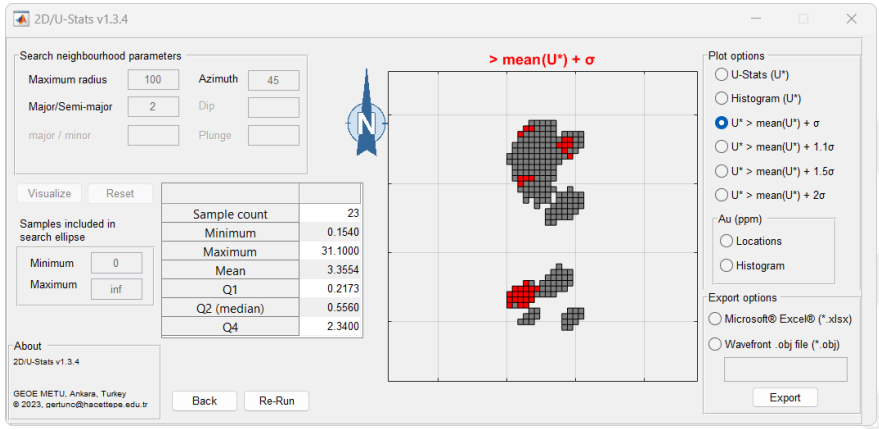
(a) U-Stats (U^*) values



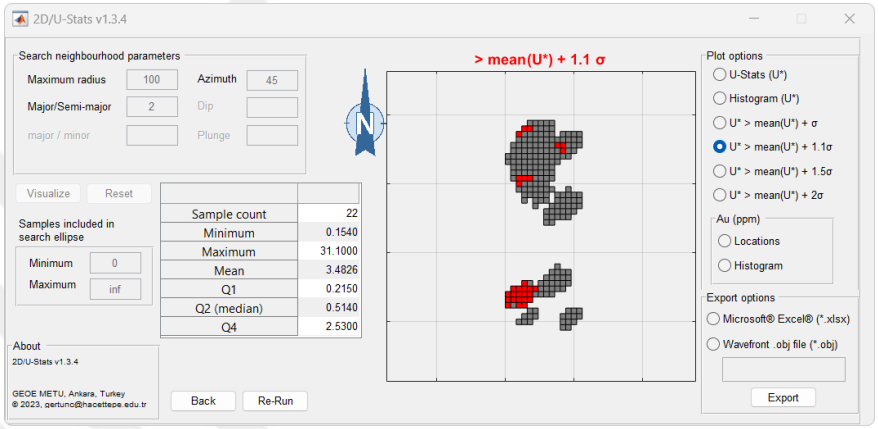
(b) Histogram of U^*

Figure 4.6: U-Stats GUI: 2D, results related plots

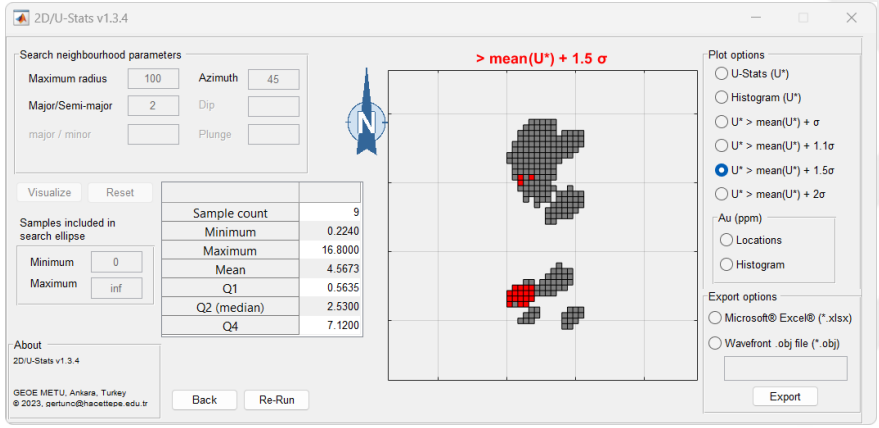
All results for the 2D case binary maps are given in Figure 4.7. Descriptive statistics windows is enabled when one of the four binary maps are selected. In this information table, statistics of samples' that are falling into blocks having value of "1" (red blocks in Figure 4.7a, 4.7b, 4.7c, and 4.7d) is given.



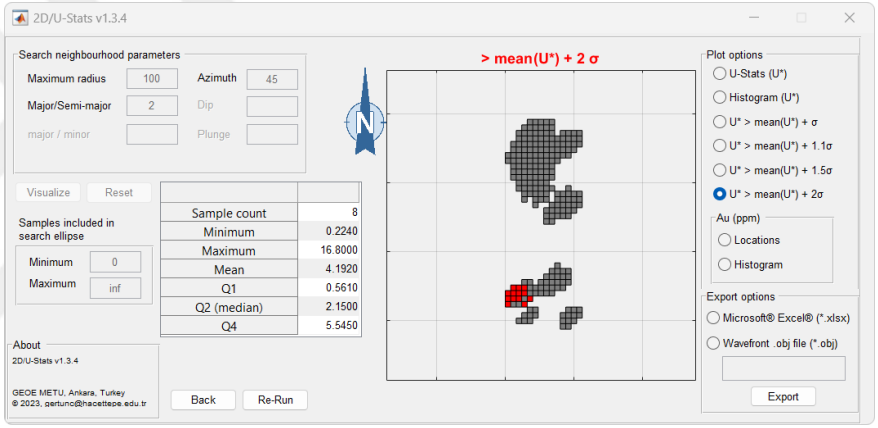
(a) mean(U^*) + σ



(b) mean(U^*) + 1.1 σ



(c) mean(U^*) + 1.5 σ



(d) mean(U^*) + 2 σ

Figure 4.7: U-Stats GUI: 2D, binary maps

Five result options (excluding the Histogram of U^*) can be exported to Microsoft® Excel® (*.xlsx). Additionally, all of the binary maps can be exported into Wavefront *.obj file format with the filename given by the user.

Figure 4.8 shows the "2D.obj" file produced with 3D/U-Stats imported into Surpac 2022 Refresh 3.

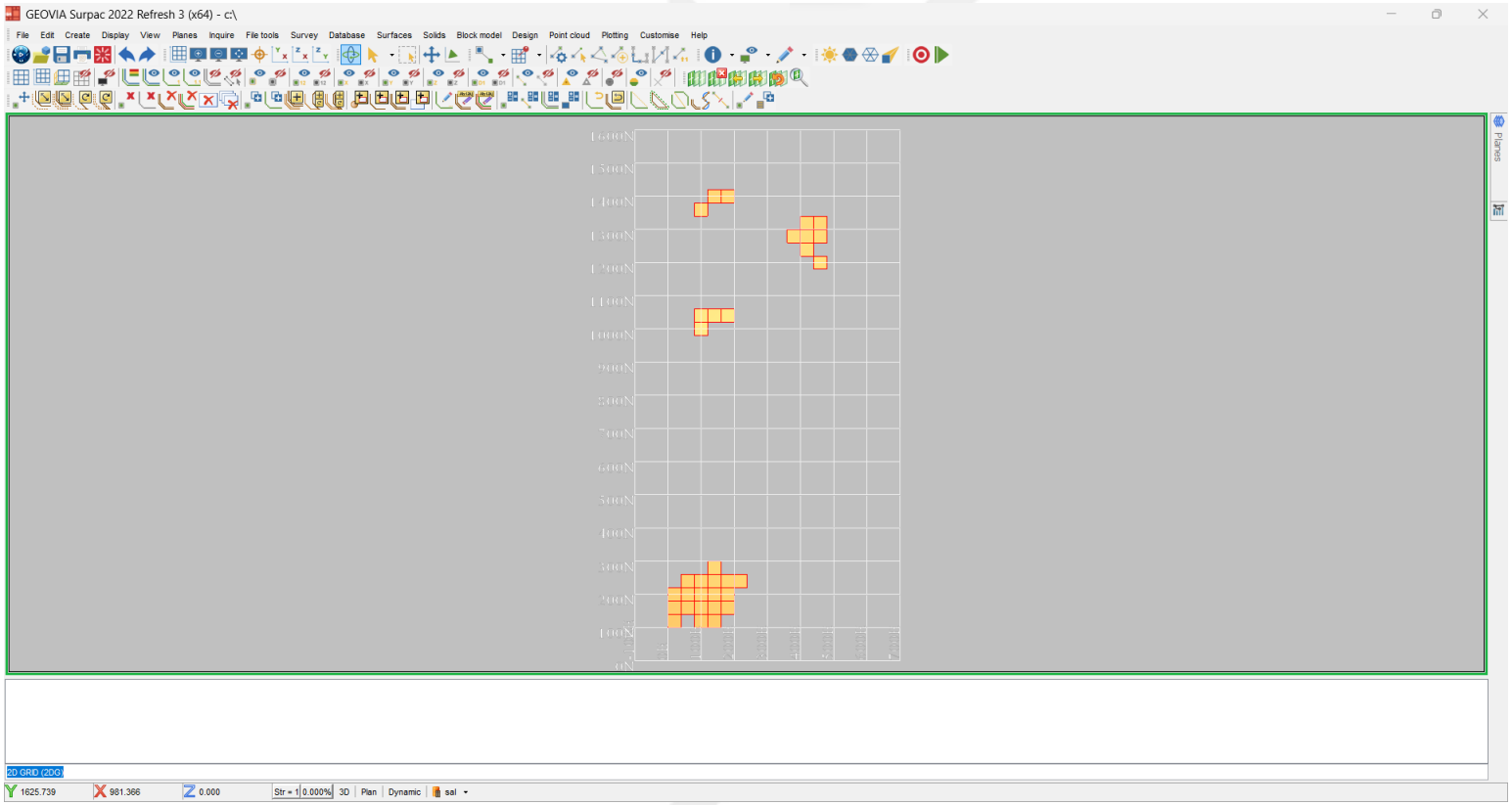


Figure 4.8: Imported "2D.obj" in Surpac 2022 Refresh 3

CHAPTER 5

U-STATS GUI: 3D

This chapter covers U-Stats GUI: 3D which can be accessed through 3D option in U-Stats GUI (Figure 5.1). In this chapter, each interface of the 3D case is demonstrated under corresponding subsections.

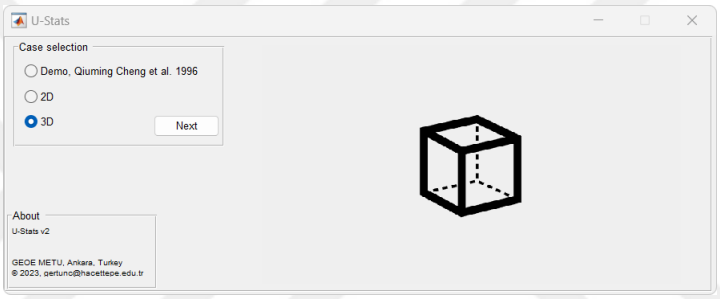


Figure 5.1: U-Stats GUI main window, 3D selection

5.1 Database Import

First interface of the U-Stats GUI: 3D is related to the database import into the program. General structure of the interfaces used in this import phase is given in detail in Figure 5.2. User starts the project by setting the "working directory". Database import starts with the collar file, which contains the borehole coordinate information. Mandatory fields in the collar file are Hole id: Name of each borehole, Easting(X): Easting coordinates of boreholes, Northing(Y): Northing coordinates of boreholes, Elevation(Z): Elevation coordinates of boreholes, and Depth: Total length of the boreholes.

In the database collar import, all fields are checked and validated for errors and the

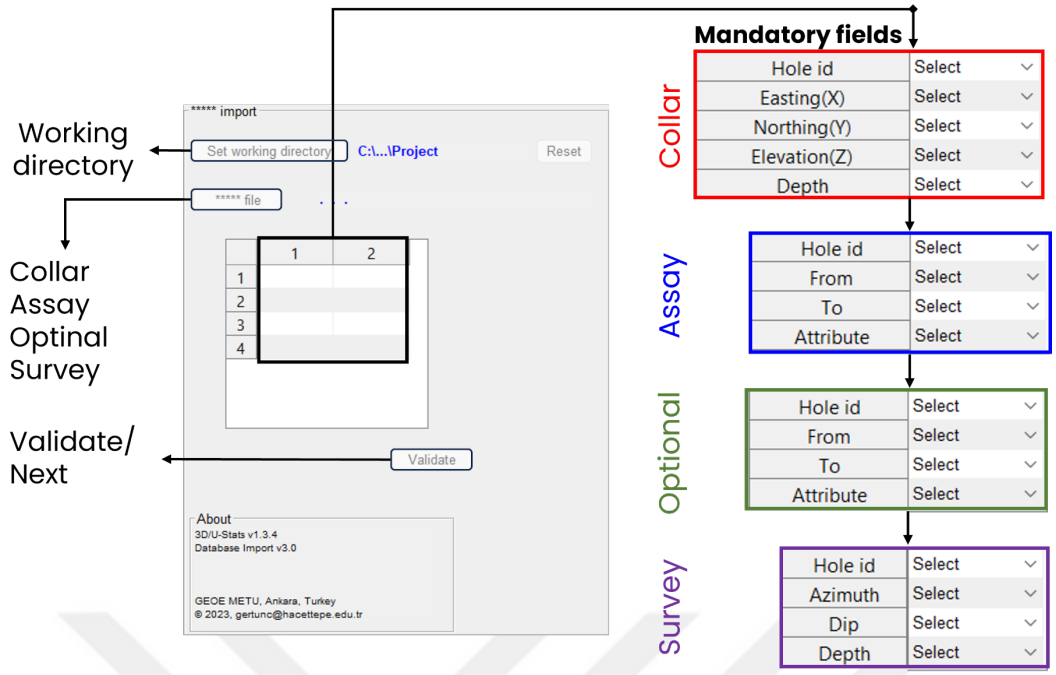


Figure 5.2: U-Stats GUI: 3D database import interface

user is notified with a report file. All fields in this import phase except hole id must be numeric, therefore, validation algorithm only reports whether coordinate values and maximum depth are numeric or not. In Hole id field, duplicates are reported. Also, blank entries are regarded as an error. The assay file cannot be loaded until all the collar fields have been verified and successfully imported.

Assay file should be in the form of intervals. This requires each assay is defined row-wise with respect to the from and to depths for the corresponding boreholes. Mandatory fields in assay file import are as follows: Hole id: The connection of the Assay file with the boreholes in the Collar file is achieved by matching the hole id column in assay file, From: Indicates starting depth of sample that is analyzed, To: end depth of sample. (i.e., difference (To-From is the sample length of corresponding assay entry), and Attribute: analyze value of the variable at interest.

Verification, validation, and error report generation process of the Assay file is more complex and diverse compared to the Collar file. Potential errors and verification routines can be listed for each mandatory field are as follows:

- Hole id: Boreholes that exist in the assay file but not in the collar file. Same

applies for the other way around. Blank entries.

- From: Nonnumerical or blank entries. Values that exceed "Depth" of corresponding borehole. Values higher than "To" values of corresponding assay entry. Duplicated "From" values.

- To: Nonnumerical or blank entries. Values that exceed "Depth" of corresponding borehole. Values lower than "From" values of corresponding assay entry. Overlapping From – To intervals. Duplicated "To" values.

- Attribute: Nonnumerical entries. The blank entries are listed as warning, not regarded as an error.

After Assay import validation, user may import optional file in order to enhance the anomaly detection. This file could contain lithology, geological domain or alteration information. In U-Stats GUI: 3D, by the aid of this file, user may constraint assay entries within the optional field. This file has identical interval structure with previous step's Assay file import. Hence, the validation routines are exactly same. If such optional file does not exist, user may skip this window via "Skip" button that appears at the beginning.

Finally, Survey file is imported. Survey file is related to the path of boreholes (vertical or directional). In order to determine borehole position, Minimum Curvature Method (MCM) is assumed as the mathematical model. By employing measured depth, dip, and azimuth as input parameters, output parameters are obtained such as Dogleg Severity (DLS) and the 3D coordinates; northing, easting, and true vertical depth. DLS is defined as an standardized estimation (degrees/100 ft) of curvature between two consecutive survey stations (Islam & Hossain, 2021; Sawaryn & Thorogood, 2005). Curvature of the directional borehole and important parameters in calculations are schematically represented in Figure 5.3.

In the first step, DLS angle β (Equation 5.1) is calculated. Here, $E_{2,1}$ and $A_{2,1}$ are dips and azimuth values of the two consecutive angle measurement points (1 and 2) in the survey file, respectively.

After calculating the DLS angle, the ratio factor (RF) is calculated with the formula

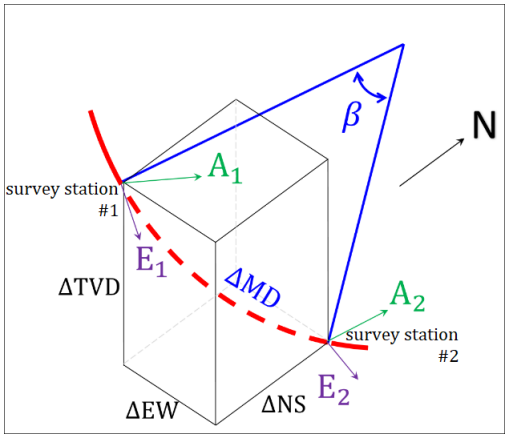


Figure 5.3: Angles used in MCM calculation and curvature of the calculated path of borehole (dashed red line)

in Equation 5.2. In the last step, the increments of the coordinate components between the angle measurement points are calculated as in Equation 5.3, 5.4, and 5.5.

$$\beta = \cos^{-1}\left(\cos(E_2 - E_1) - sin(E_1) \times sin(E_2) \times (1 - \cos(A_2 - A_1))\right) \tag{5.1}$$

$$RF = \frac{2\left(\frac{\beta}{2}\right)}{\beta} \tag{5.2}$$

$$\Delta NS = \frac{\Delta MD}{2} \times \left(\sin(E_1) \times \cos(A_1) + \sin(E_2) \times \cos(A_2)\right) \times RF \tag{5.3}$$

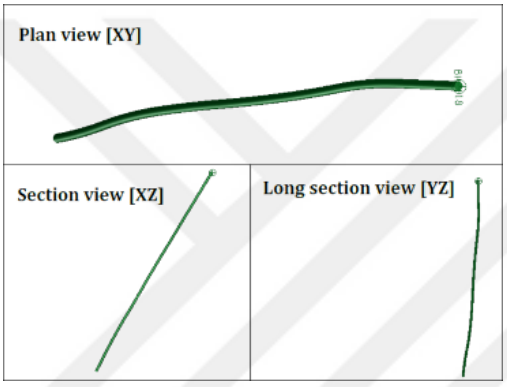
$$\Delta EW = \frac{\Delta MD}{2} \times \left(\sin(E_1) \times \cos(A_1) + sin(E_2) \times \sin(A_2)\right) \times RF \tag{5.4}$$

$$\Delta TVD = \frac{\Delta MD}{2} \times \left(\cos(E_1) - cos(E_2)\right) \times RF \tag{5.5}$$

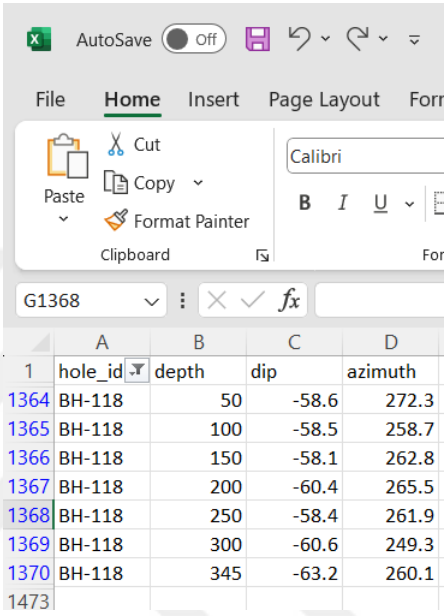
where, ΔNS: Northing, ΔEW: Easting, and ΔTVD: Elevation increment, respectively. ΔMD refers to the distance between two survey stations.

Further detailed information is well documented and can be referred from Ertunç and İmer, 2022 (in Turkish).

Majority of the boreholes in industrial practice are directional. Directional boreholes are defined by varying dip and azimuth values at corresponding depths. Single directional borehole, namely BH-118, is visualized in Figure 5.4 as an example. Figure 5.4a and 5.4b shows section views of the BH-118 and the portion of survey csv file.



(a) Sectional views of BH-118



	A	B	C	D
1	hole_id	depth	dip	azimuth
1364	BH-118	50	-58.6	272.3
1365	BH-118	100	-58.5	258.7
1366	BH-118	150	-58.1	262.8
1367	BH-118	200	-60.4	265.5
1368	BH-118	250	-58.4	261.9
1369	BH-118	300	-60.6	249.3
1370	BH-118	345	-63.2	260.1
1473				

(b) Survey entries of BH-118

Figure 5.4: Borehole BH-118

Correct database import is vital phase of the algorithm since all of the remaining steps are built with respect to the assay values' coordinates. In order to check correctness of import, the program is tested with realistic 3D scenario. The results of imported middle assay coordinates of the U-Stats GUI: 3D are compared with GEOVIA Surpac™. GEOVIA Surpac™ academic licence is acquired from Hacettepe University, Department of Mining Engineering (Surpac 2022 Refresh 3).

Figure 5.5 shows scatter plot of each coordinate components (Northing(Y), Easting(X), and Elevation(Z)) of assay entries. From the results it can be seen all of the components are identical. Equation of the trendlines are obtained as y=x and correlation coefficients are equal to 1 (r=1).

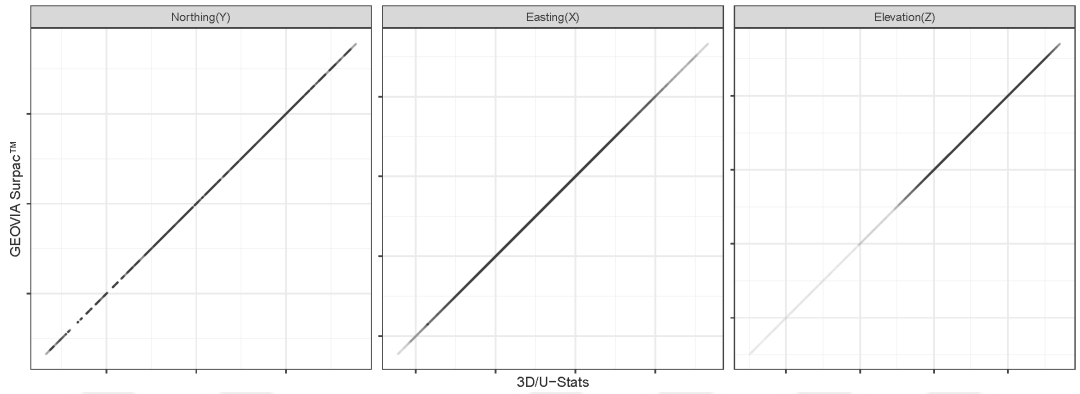


Figure 5.5: Scatter plot, U-Stats GUI: 3D vs GEOVIA Surpac™ coordinates

5.2 Base Map

Following database import, base map of the boreholes are displayed in Base Map window (highlighted in black dashed, Figure 5.6), providing user a visual check whether the database is properly imported or not. Information about borehole database is located on the top-right of the panel.

In Base Map window, user may export in three formats (highlighted in cyan, Figure 5.6). They are Microsoft® Excel® (*.csv), GEOVIA Surpac™ (*.str), and GeoEAS (SGemS) format, respectively. When the boreholes are colored by "Drillholes", only option to export is GEOVIA Surpac™ (*.str) and in this file collar of boreholes (i.e. coordinate components of boreholes (x, y, z), hole_id, and maximum depth is included.

Second option in main plot of base map is color by Attribute (highlighted in orange, Figure 5.6). In this visualization option, there is an "Plot options" panel for the color palette, low and high bound values of the attribute colored in the thematic map, and constraint based on the optional file's attribute (highlighted in red and blue, respectively, Figure 5.6). The color palette (highlighted in green, Figure 5.6) is adapted

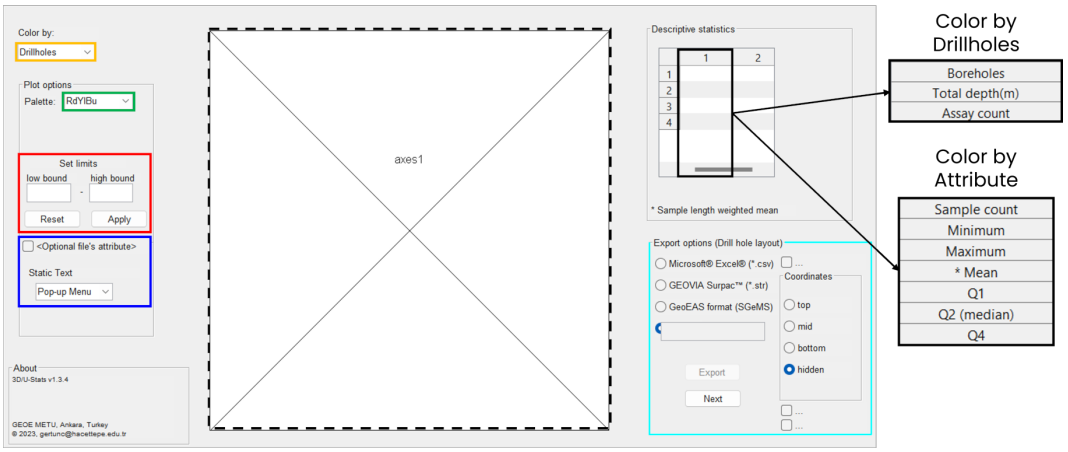


Figure 5.6: U-Stats GUI: 3D, base map interface

from RColorBrewer (Neuwirth, 2022) from the R software package (R Core Team, 2023). There are 5 options, all of which are colorblind safe. These are RdYlBu: Red Yellow Blue, RdBu: Red Blue, PuOr: Purple Orange, PuOr: Purple Red Green. In this option, all 3 export options are available. There are up to 12 field that can be exported. Coordinate components are available as follows: "(x,y,z)_from" assay beginning coordinates, "(x,y,z)_to" sample end coordinates, and "(x,y,z)" sample middle coordinates. In addition, "hole_id", "sample length", and "attribute" values are also available as an export fields.

5.3 Digital Elevation Model Import

In U-Stats GUI: 3D, like all conventional mining software packages, the Digital Elevation Model (DEM) is used to determine the separation between air (above DEM) and target locations (below DEM) for following calculations. The input format of DEM is ASCII without delimiter restrictions. The point cloud represented in Northing(Y), Easting(X), and Elevation(Z) columns are called and loaded from the working directory. When the DEM is loaded into the program, the topography is visualized in the module window (Figure 5.7) with orange point cloud together with borehole paths. The aim of this visualization is to guarantee that the user properly loaded the DEM along with borehole data.

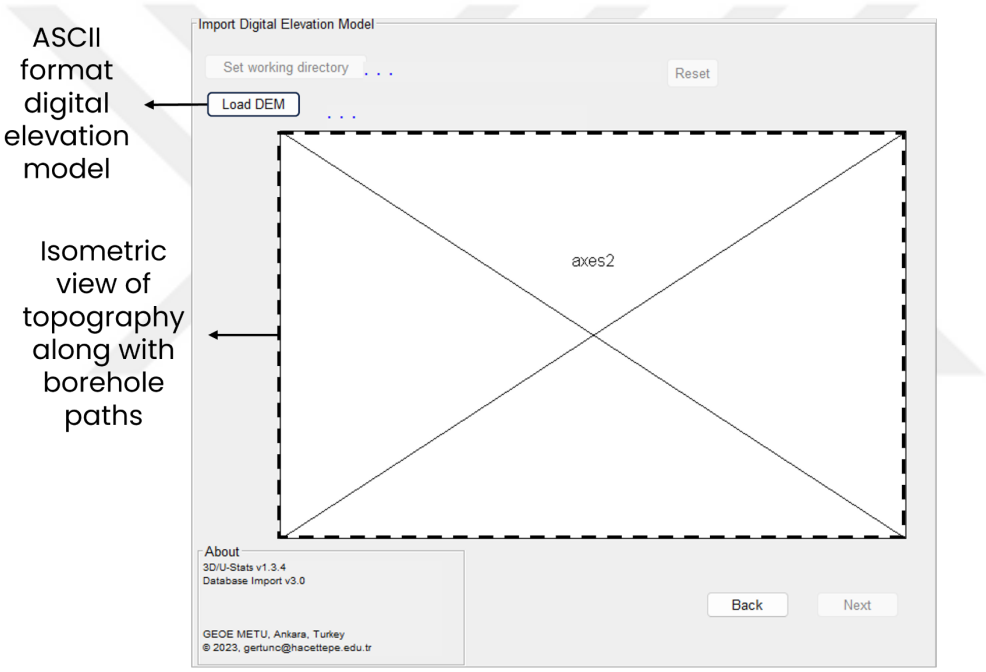


Figure 5.7: U-Stats GUI: 3D, digital elevation model import interface

Following step is to define target locations. With "Next" button, "Target Locations" windows is opened.

5.4 Target Locations

The target location module has nine edit boxes that the user must enter into the program (highlighted in red, Figure 5.8). These are the minimum value for each coordinate component (easternmost, westernmost, and lowest elevation coordinate values for Y, X, Z, respectively), the extent of the 3D mesh grid, and the target grid sizes in each direction. When the model is created, the target grid centroids are visualized as a point cloud together with the DEM in the module window. By default, the target location module applies the "mesh grid not above DEM" constraint to mesh grid automatically, based on the DEM loaded in previous step (5.3 Digital Elevation Model Import). Any mesh grid centroid created above DEM is discarded.

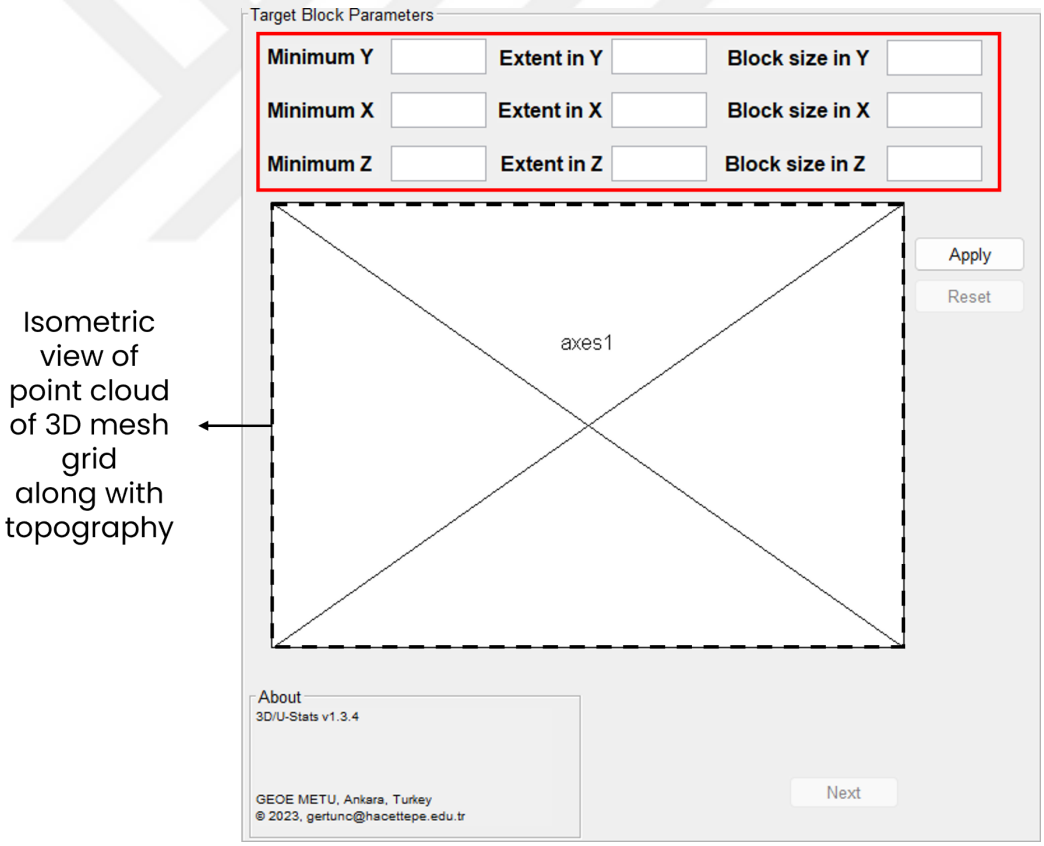


Figure 5.8: U-Stats GUI: 3D, target locations interface

5.5 Search Ellipsoid

Search Ellipsoid window of the U-Stats GUI: 3D is an adaptation from 3D geostatistics application compiled by the author (unpublished). The U-Stats methodology does not need variogram parameters as in geostatistics. Therefore, variogram related parameters are disabled and greyed out (Figure 5.9).

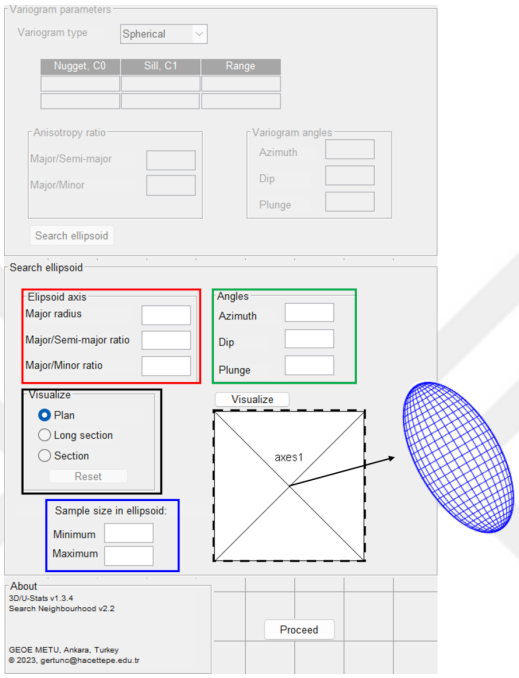
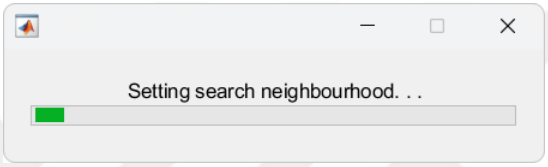


Figure 5.9: U-Stats GUI: 3D, search ellipsoid interface

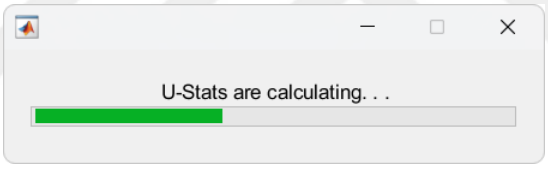
"Ellipsoid axis panel" is related to the geometric aspects of the ellipsoid (highlighted in red, Figure 5.9). Major radius, as the name implies, is the longest axis. Major/Semi-major and Major/minor ratios are for the calculation of other radii lengths. "Angle" panel defines the orientation of the ellipsoid (highlighted in green, Figure 5.9). In "Visualize" panel, user may visualize ellipsoid in three major axis (Plan, Long section, and Section) (highlighted in black, Figure 5.9). The "Minimum" and "Maximum" sample size in ellipsoid defines the minimum and maximum number of samples to be included in the ellipsoid, respectively (highlighted in blue, Figure 5.9). If there are more samples than the maximum sample size in the ellipsoid, the algorithm selects the closest samples according to their euclidean distances from the ellipsoid center with the "nearest neighbour" routine.

5.6 Run

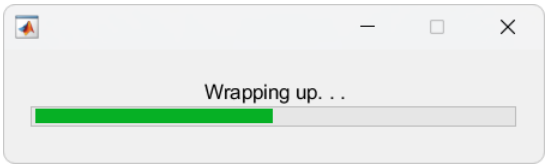
U-Stats GUI: 3D run has three phases. In the first phase, samples are filtered for the each target location defined in previous step. Target locations that cannot meet the sample size selection criteria (defined in 5.5 Search Ellipsoid) are not taken into consideration. Progress bar for this step is shown in Figure 5.10a. Second phase is the main engine for the U-Stats calculations. Users are notified with the progress bar Figure 5.10b. When the calculations are done, "Wrapping up" sub-routine is called (Figure 5.10c). In this phase, suitable column-wise blocks are merged together in order to relax graphical handling of the GUI in the cases of large target locations. In this case block size in Z direction are summed up.



(a) Sample selection



(b) Run



(c) Reducing blocks in progress

Figure 5.10: U-Stats GUI: 3D, progress bars

5.7 Results

After calculations are completed, algorithm transforms U-Stats (U^*) values into binary variables based on the thresholds mean(U^*) + σ, mean(U^*) + 1.1 σ, mean(U^*)

+ 1.5 σ, and mean(U^*) + 2 σ (highlighted in red, Figure 5.11). Multipliers of the standard deviation σ can be considered as confidence levels, just like the confidence interval in statistics. Target locations having U^* greater than threshold labeled as "1" and rest of the locations ($U^* \leq$ mean(U^*) + $\times$ σ) are "0". On the top-right panel, descriptive statistics of the assay values which fall inside resulting 3D mesh grid are presented (highlighted in black, Figure 5.11). Users may re-run the U-Stats GUI: 3D by "Re-run" button. This button redirects to Search Ellipsoid (Section 5.5). If users desire to change target locations 3D mesh grid size and/or the low-high bound limits of the attribute (i.e. input assays) and then re-run, this can be achieved via Back to Base Map (Section 5.2) button.

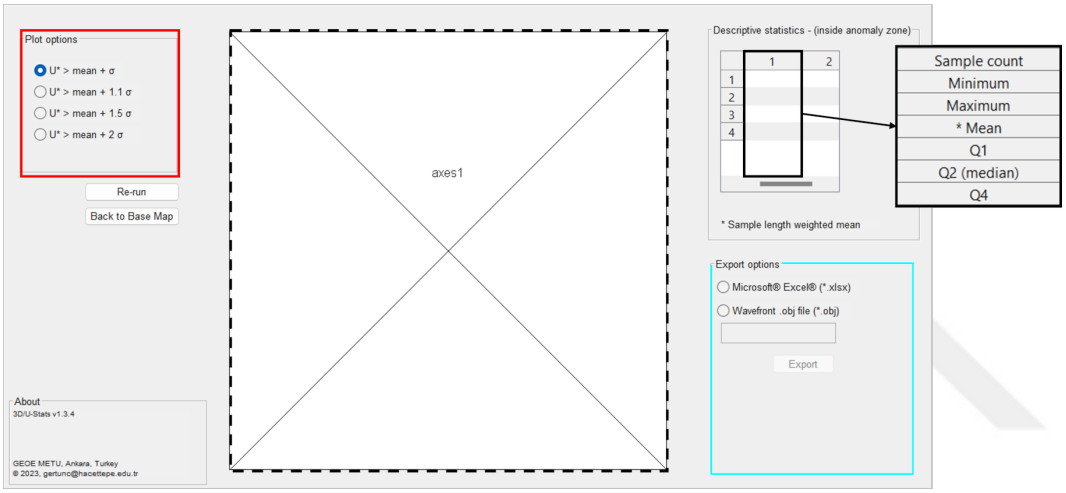


Figure 5.11: U-Stats GUI: 3D, results interface

Results can be exported in two formats. First available format is Microsoft® Excel® (*.xlsx) (highlighted in cyan, Figure 5.11).

CHAPTER 6

CASE STUDIES

This chapter includes U-Stats GUI: 3D case studies for the Salınbaş and Taç mineralizations. Before solutions, comprehensive exploratory data analysis of both mineralizations are presented.

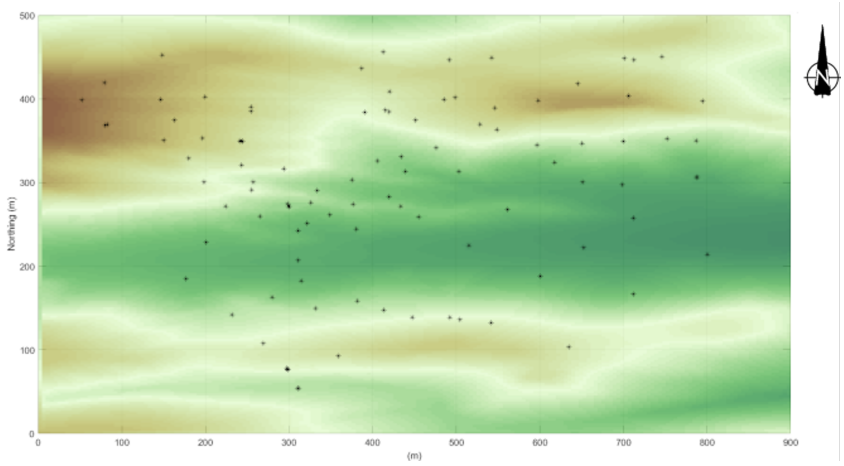
The content and organization of this chapter are as follows:

- In Section (6.1), the elevation map and the collar map of the borehole databases are given. Additionally, summary statistics, histograms of core sample lengths with Au (ppm) attribute, and cumulative frequency plot for threshold values for outliers and clusters are included.
- Section 6.2 covers all interfaces of the U-Stats GUI: 3D with Salınbaş Au (ppm) database.
- Section 6.3 presents only solution-related and result screens for the Taç Au (ppm) database since majority of the interface steps are similar with the previous Section 6.2.

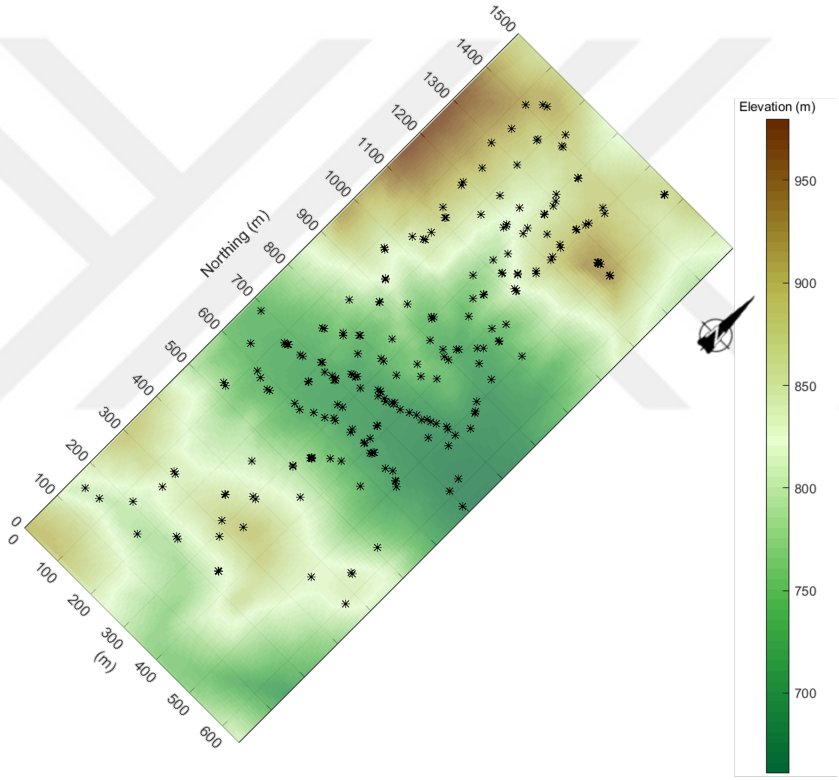
6.1 Exploratory Data Analysis

The Salınbaş and Taç databases include 102 and 234 boreholes, respectively, which were utilized in the case studies of the thesis. In Salınbaş, there are 42 vertical boreholes and 60 directional boreholes, whereas in Taç, 11 are vertical and 223 are directional. As of this version, U-Stats: 3D program produces solutions based on univariate input. Although multi-element analyses are included in the databases in the

case studies, only the Au variable (unit is in ppm) was used within the scope of the thesis study. The total length of boreholes in Salınbaş and Taç databases is 11302 and 50687 m, respectively. The elevation maps of topographies together with the borehole collars of two mineralizations are given in the Figure 6.1. The bounded areas in the case studies are 45 and 90 hectares for Salınbaş and Taç, respectively.



(a) Salınbaş



(b) Taç

Figure 6.1: Elevation map & borehole collars for a) Salınbaş and b) Taç projects

Descriptive statistics of Au (ppm) from both mineralizations are summarized in Table 6.1. Total number of assay entries for the Au (ppm) attribute are 6280 and 42903 for the Salınbaş and Taç mineralizations, respectively.

Table 6.1: Descriptive statistics of Au (ppm) from both mineralizations.

	Mineralization	
†Au (ppm)	Salınbaş	Taç
Count	6280	42903
Minimum	0.003	0.005
Maximum	44.5	895.6
‡Mean	0.233	0.324
Q1	0.006	0.024
Q2 (median)	0.026	0.054
Q3	0.104	0.129
Variance	2.473	60.8

† Salınbaş and Taç lithogeochemical data courtesy of Zenit Madencilik and Santral Madencilik, respectively.

‡ length weighted

From the summary statistics, it can be seen that Taç Au (ppm) has larger range (895.595 ppm) than Salınbaş Au (ppm) (44.497 ppm). When the IQR's (IQR=Q3-Q1) of the two attributes are compared, it is seen that they vary in a similar range. This value is 0.098 ppm for Salınbaş and 0.105 ppm for Taç. When the histograms of sample lengths are examined (Figure 6.2), it can be seen that the core sampling strategy in the drilling campaigns carried out in both fields is similar. According to the relative frequencies in both histograms, approximately 60% of the core sample lengths are 1 and 2 m. This may have caused the length-weighted means (for Salınbaş and Taç 0.233 ppm and 0.324 ppm, respectively) to not be very different from each other.

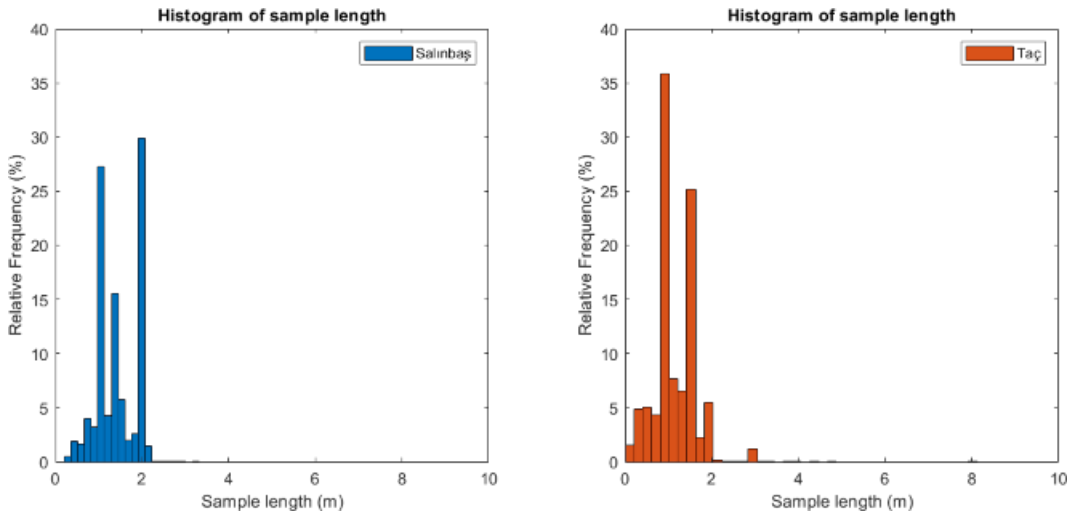


Figure 6.2: Histogram of Au (ppm) sample lengths from Salınbaş and Taç databases.

Histograms of the Au (ppm) attribute are given in Figure 6.3. It is known that there are outliers in Au values in both databases. Therefore, it is natural that the histograms of the raw data show right skewed distribution (blue bars in Figure 6.3: raw). However, in this case, it is very difficult to examine the distribution of the data due to the large difference between background as well as low grade Au values and relatively higher Au grades. Therefore, the raw data was converted to the base 10 logarithm and the histogram of the log(Au (ppm) variable was drawn (red bars in Figure 6.3: log transformed).

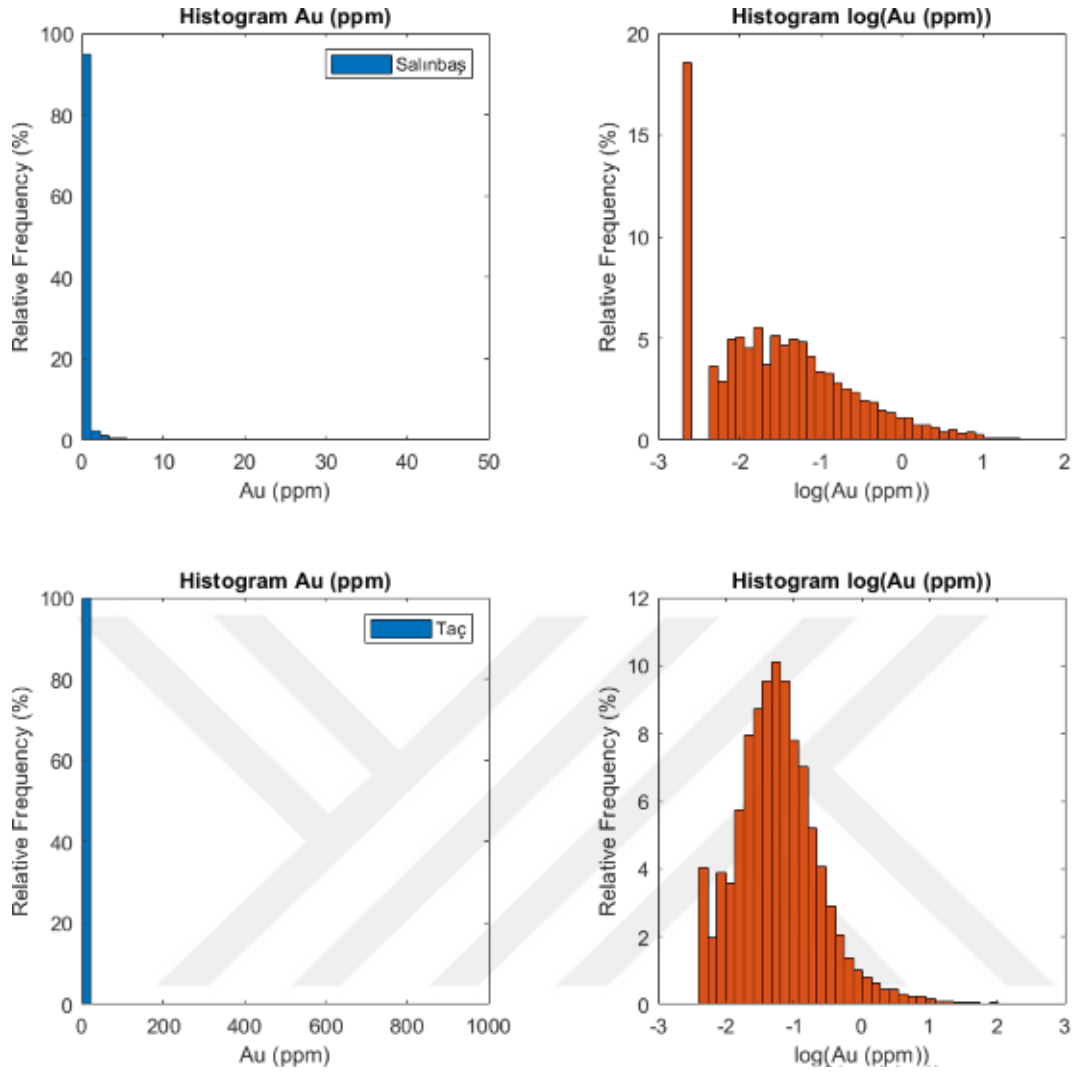


Figure 6.3: Histogram of Au(ppm) and log(Au(ppm)) from Salınbaş and Taç databases

When the log transformed histograms are examined, it is seen that the Au attributes of the Salınbaş and the Taç field exhibit distributions with different characteristics from each other. Both log transformed distributions are not log-normal but while the relative frequency peak is more prominent in Salınbaş, this peak is not observed in Taç.

Within the scope of the thesis study, outlier values were only examined statistically. For this purpose, cumulative frequency distribution plots were drawn and visualized in Figure 6.4.

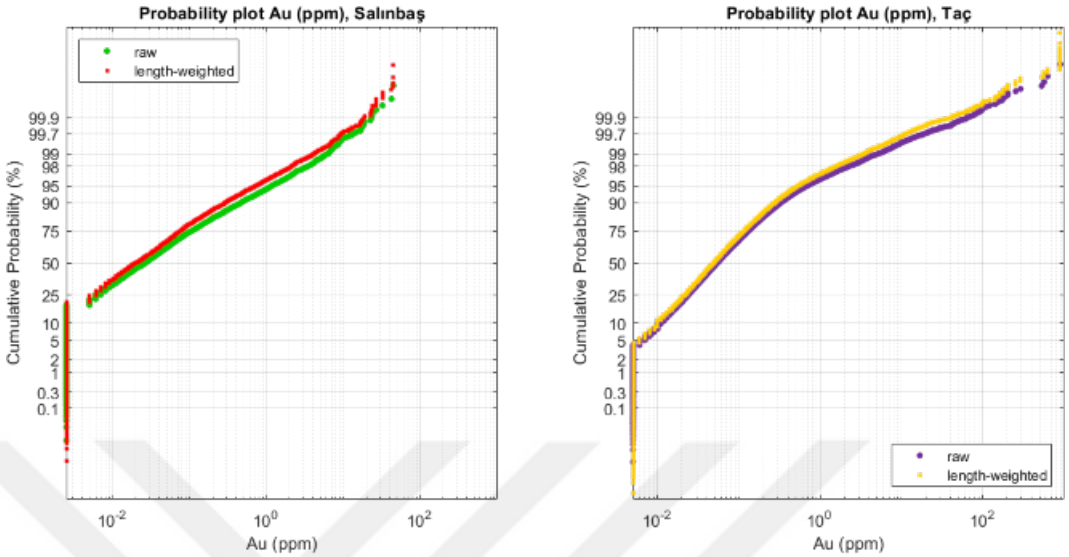
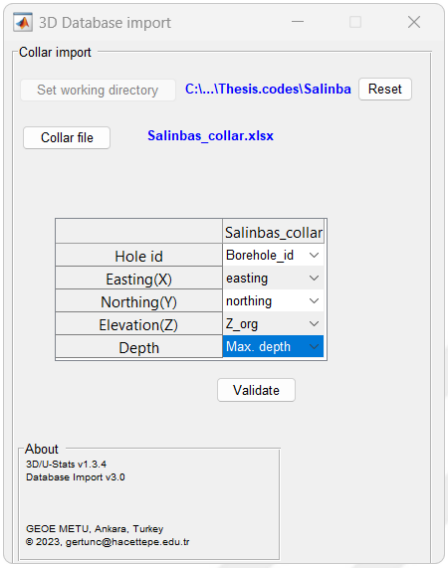


Figure 6.4: Cumulative probability plots of Au (ppm) from Salınbaş (left) and Taç (right) databases. Plots were prepared both for raw and length-weighted data.

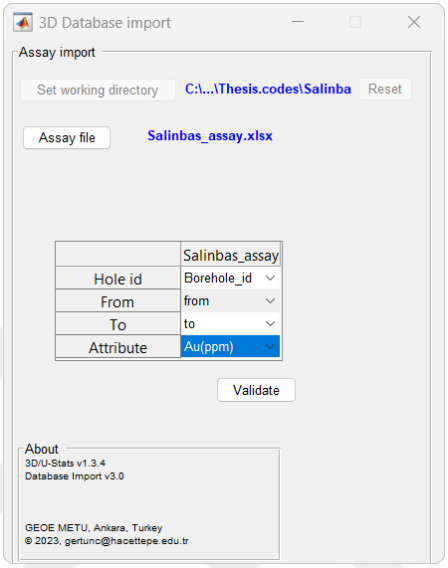
From cumulative probability distributions, threshold values of Au for outlier detection can be seen heuristically. In cumulative probability graphs, saddle points generally mean threshold values for possible clusters. When these saddle points for Salınbaş and Taç graphs are examined, the two fields have different characteristics from each other in terms of how clearly the clusters are separated from each other.

6.2 Case Study: Salınbaş Mineralization

In the first stage of U-Stats GUI: 3D, a total of 103 boreholes in the Salınbaş case study, 6250 assay values obtained from these boreholes, and the survey file for directional boreholes were imported into the program (Figure 6.5). In this case study, the optional file was not used and this import step was skipped (Figure 6.5c).



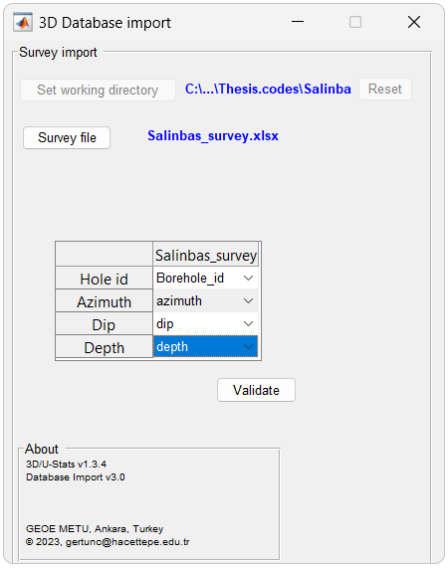
(a) Collar file



(b) Assay file



(c) Optional file



(d) Survey file import

Figure 6.5: Salınbaş database import

In the Figure 6.6, Au (ppm) attributes are constrained between 0.0025 and 0.24 ppm. Sample count, minimum, maximum, sample length weighted mean, Q1 (first quartile), Q2 (second quartile or median) and Q3 (third quartile) statistical parameters for this interval are included in the descriptive statistics panel at the top-right panel.

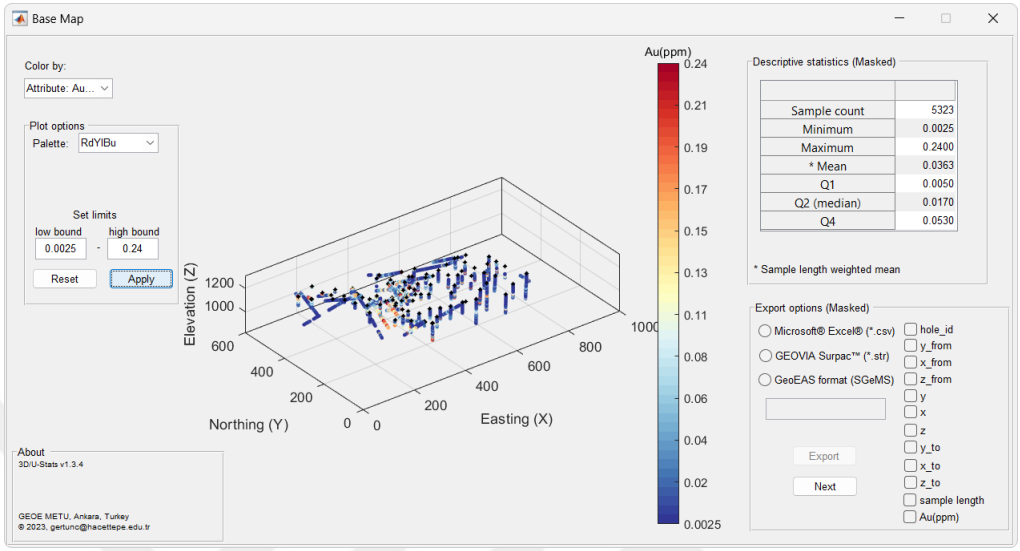


Figure 6.6: U-Stats GUI: 3D, Salınbaş base map, color by Au (ppm)

In the following step, DEM is imported from the interface. Figure 6.7 shows imported topography point could with the borehole paths.

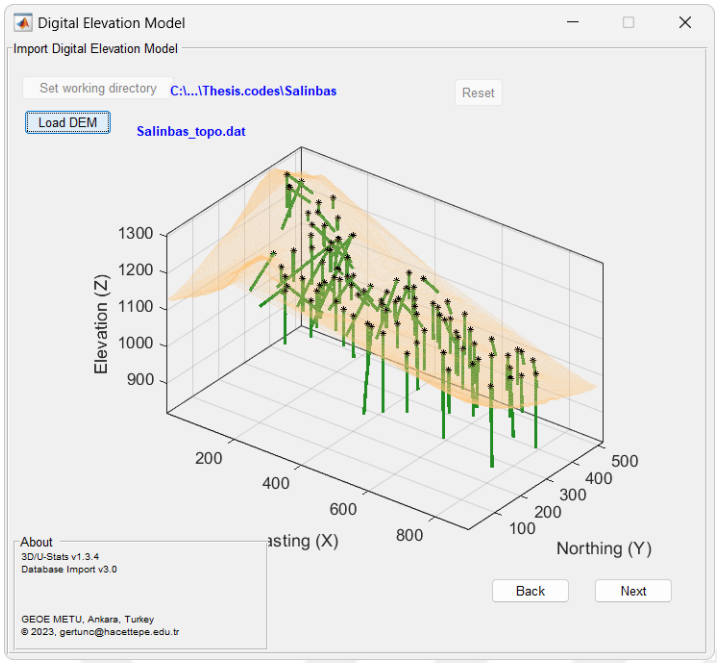


Figure 6.7: 3D digital elevation model import for Salınbaş

Mesh grid size for the Salınbaş case study is selected as 25, 25, and 5 m for northing, easting, and elevation, respectively.

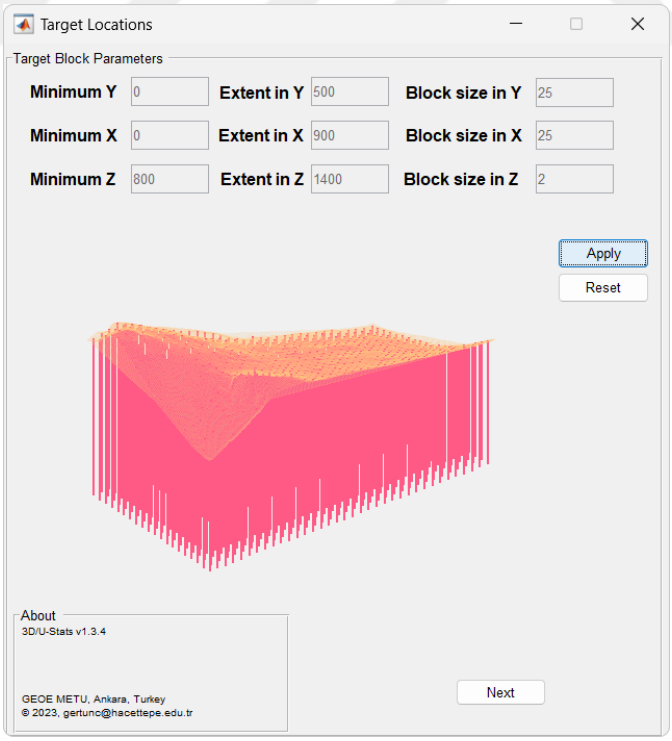


Figure 6.8: 3D mesh grid for Salınbaş

Search strategy for this case study is given in Figure 6.9. Search ellipsoid's maximum radius is set to 50 m and its anisotropy ratio is equal to 0.5. For the ellipsoid's angle, orientation setting is selected as follows: 90°, 20° for azimuth and dip angle, respectively. The plunge angle is set to 0°.

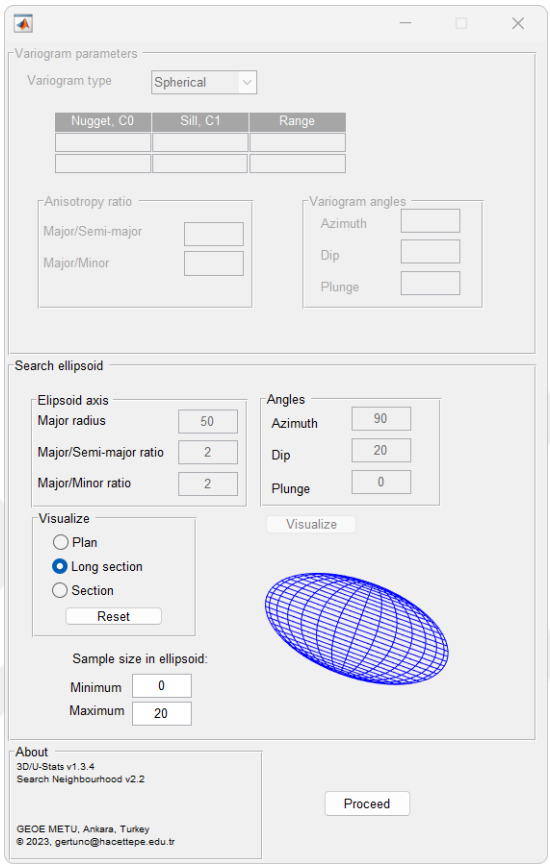
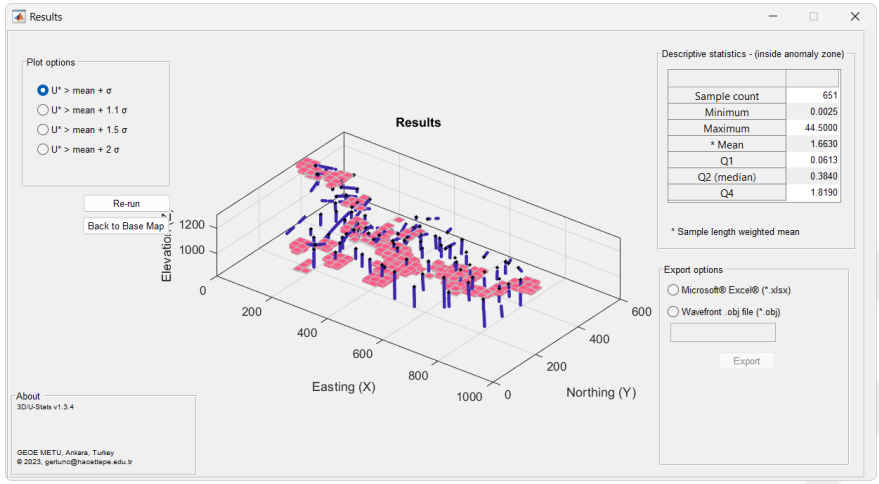


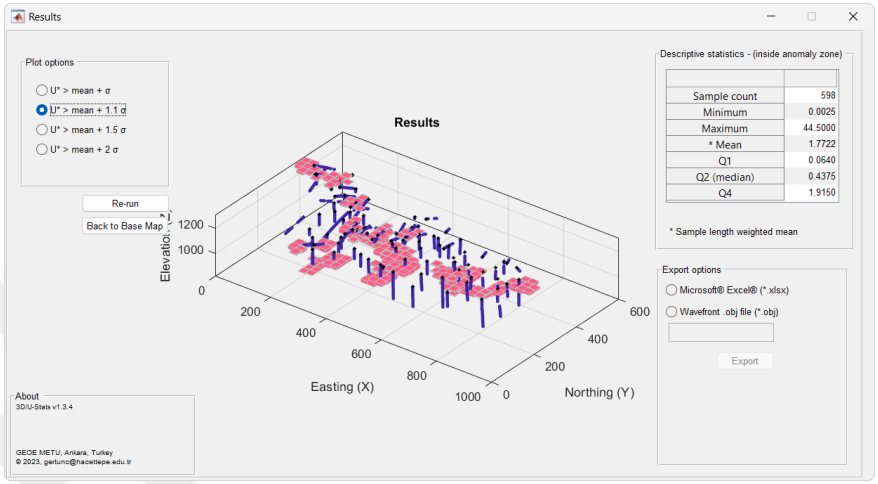
Figure 6.9: Salınbaş search ellipsoid

Number of samples included in the ellipsoid is varying in [0 - 20] interval.

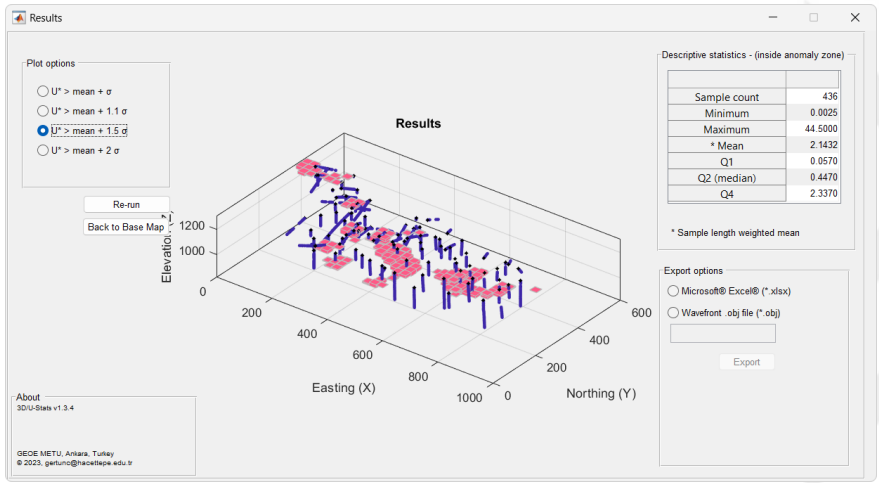
After run is completed, result screen appears. In Figure 6.10 binary maps of the results are given. The results obtained according to different σ values' descriptive statistics are given in Table 6.2.



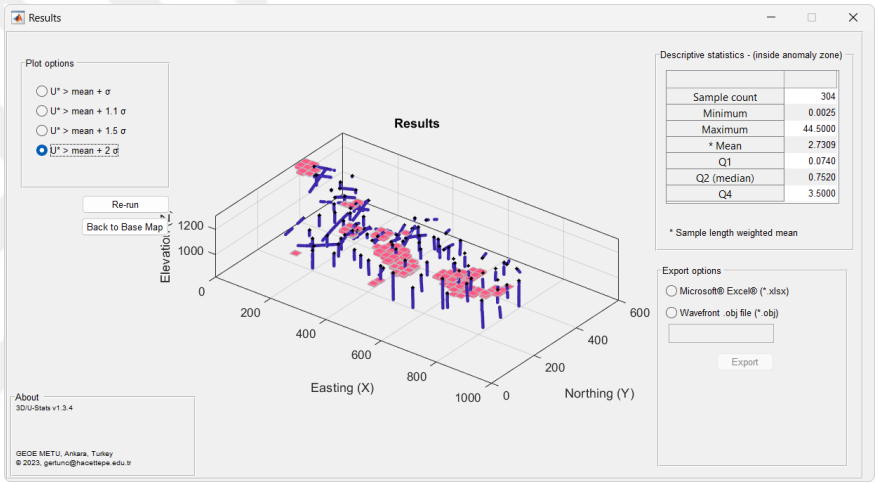
(a) mean(U^*) + σ



(b) mean(U^*) + 1.1 σ



(c) mean(U^*) + 1.5 σ



(d) mean(U^*) + 2 σ

Figure 6.10: U-Stats GUI: 3D, Salınbaş results

Table 6.2: Results comparison of different multipliers of standard deviations in Salınbaş mineralization

	U*>mean(U*) +			
	σ	1.1 σ	1.5 σ	2 σ
†Sample count	651	598	436	304
Minimum	0.003			
Maximum	44.5			
‡Mean	1.663	1.772	2.143	2.731
Q1	0.061	0.064	0.057	0.074
Q2 (median)	0.384	0.438	0.447	0.752
Q3	1.819	1.915	2.337	3.5

† samples fall inside 3D mesh grid

‡ length weighted

According to the results in Table 6.2, the minimum and maximum values of the samples falling inside the geochemical anomaly zone are same for all sigma values. These cells are given as merged in the Table 6.2. As a result of increasing sigma multipliers (1, 1.1, 1.5, and 2), the number of samples falling inside geochemical anomaly zone decreases, as expected. When the length-weighted means are examined, this mean value tends to increase for increasing sigma values. When all raw data was examined, the length-weighted mean value was 0.233 ppm (Table 6.1), while for 2σ this value was determined as 2.731 ppm. When the Q3 values (which is described as 75th percentile) of the raw data and the samples inside the geochemical anomaly zone are compared, it is seen that the values of the geochemical anomaly samples are higher.

Figure 6.11 shows the plan view, re-scaled, and clipped version of the Figure 6.10d solution (Figure 6.11 A) together with the projection of the true width $\times$ Au (ppm) attribute in the limestone contact (Figure 6.11 B), from Groves et al., 2017 for Salınbaş mineralization. The reason for re-scaling A in Figure 6.11 is to make the two plots comparable. As can be seen from Figure 6.11, the output of the program are compatible with these contours.

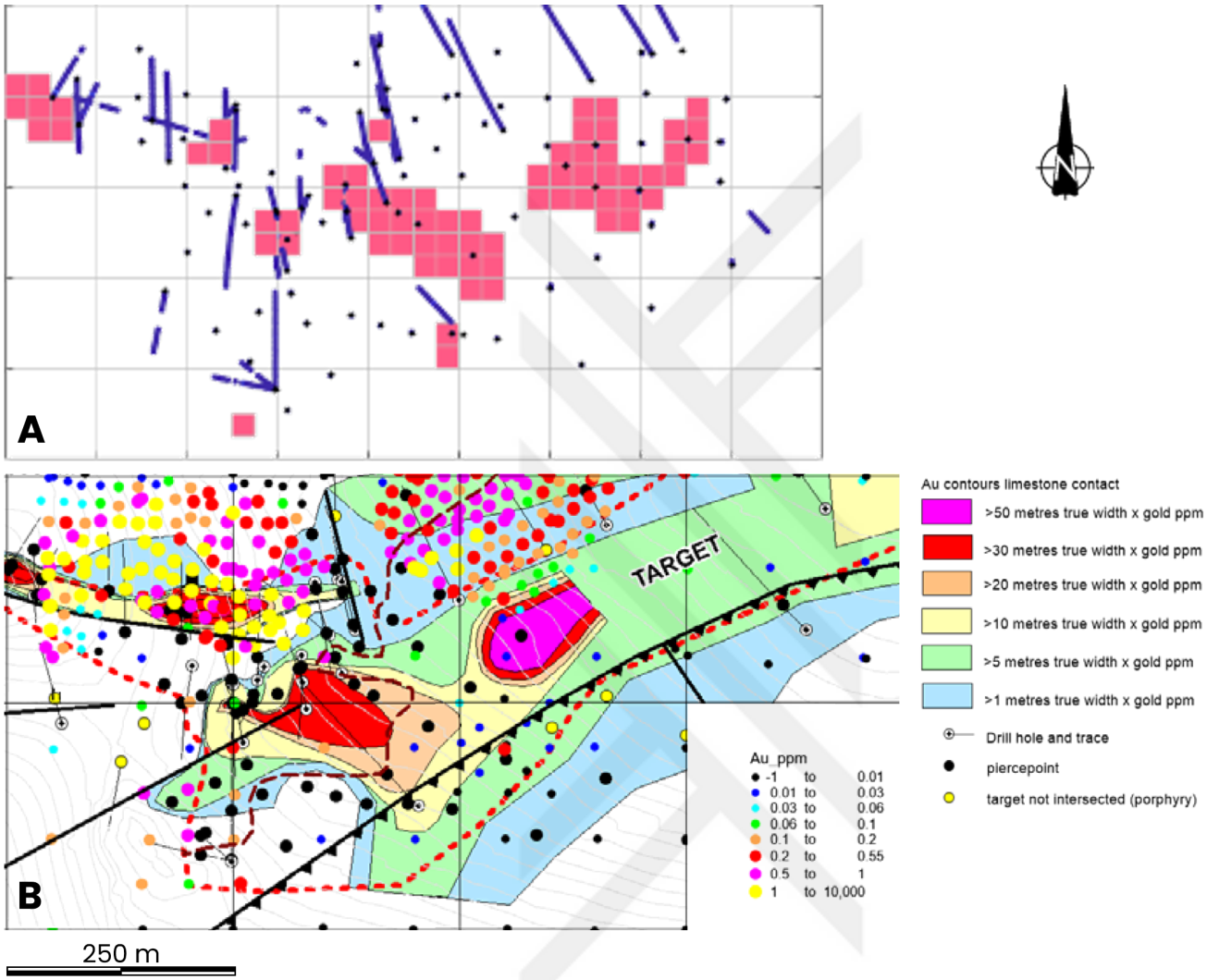


Figure 6.11: A: Plan view of geochemical anomaly zone output of 3D U-Stats, B: Au contours limestone contact. A and B are in same scale. B is modified from Groves et al., 2017

6.3 Case Study: Taç Mineralization

In the database import of Taç mineralization, the "Alteration" optional file was used, unlike the one in Salınbaş (Figure 6.12). This is because the relationship between different hydrothermal alteration styles and mineralization are better constrained during field studies in the Taç project area. At Taç, argillic alteration is widespread along the faulted corridor hosting epithermal-style mineralization. However, most mineralized veins are spatially associated with zones of silicification. As a result, this alteration type is used as another attribute during evaluation of the Tac borehole data.

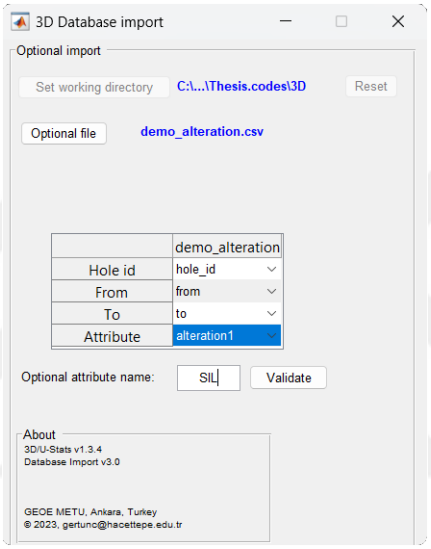
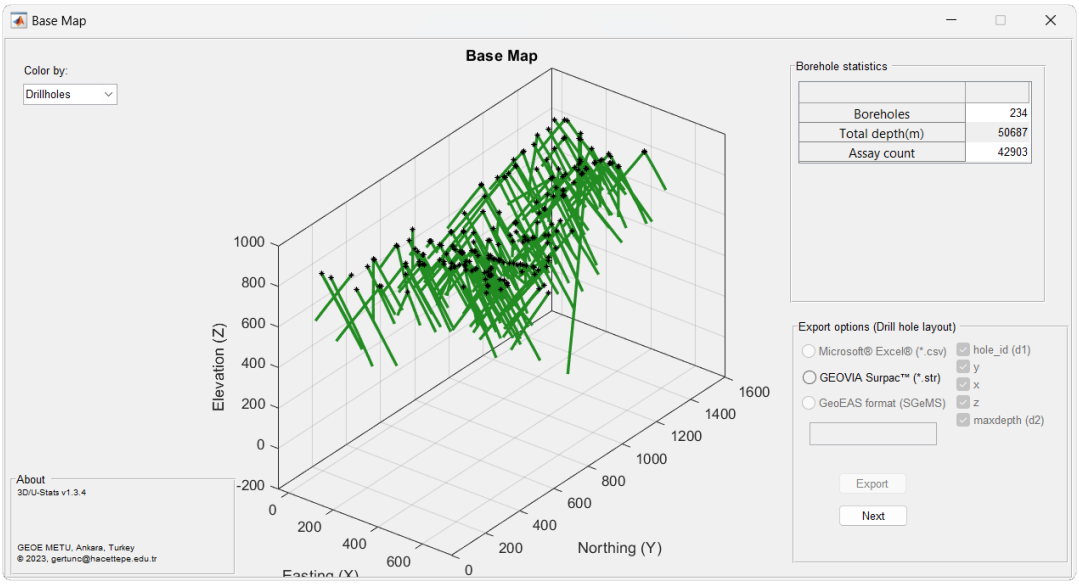
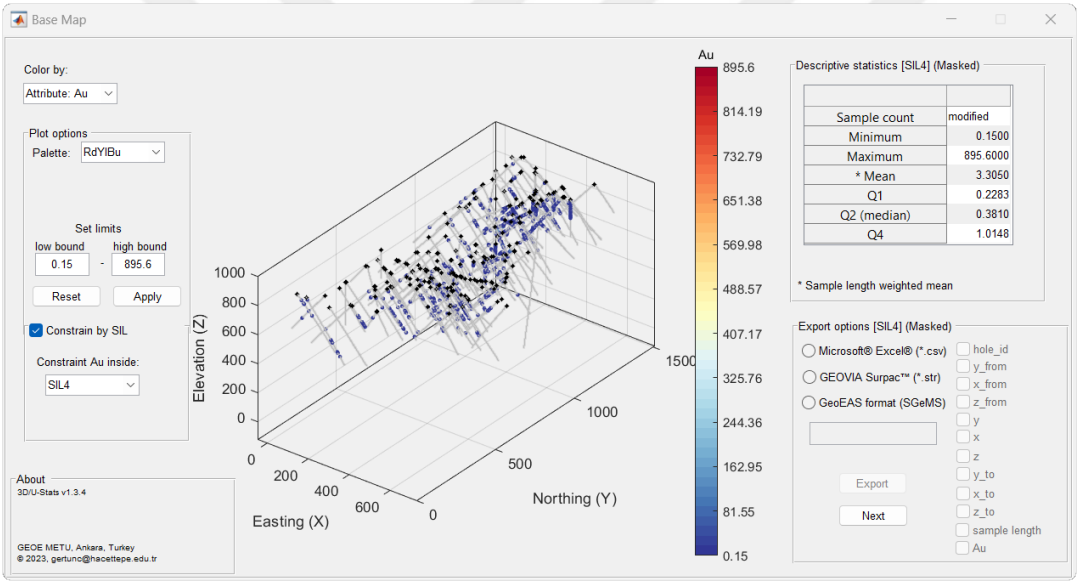


Figure 6.12: Taç database, alteration optional file import

In the Figure 6.13, Taç base maps are presented. Borehole paths' base map is given in Figure 6.13a. Au (ppm) attributes that fall within the "SIL1" attribute of the "SIL" optional file are constrained and plotted in Figure 6.13b. Sample count, minimum, maximum, sample length weighted mean, Q1 (first quartile), Q2 (second quartile or median) and Q3 (third quartile) statistical parameters are included in the descriptive statistics panel at the top-right panel. The sample count is denoted as "modified". The reason for this is the pseudo samples as a result of merging different intervals of optional and assay files.



(a) Color by boreholes



(b) Color by Au (ppm)

Figure 6.13: U-Stats GUI: 3D, Taç base map

Sample selection search strategy for the Taç run is as follows: Maximum radius of search ellipsoid is 25 m. Major/Semi major and Major/Minor anisotropy ratios are set to 1 and 2, respectively. Ellipsoid has a dip angle of 30°. Sample size is varying in between 3 and 16. The search ellipsoid interface is given in Figure 6.14.

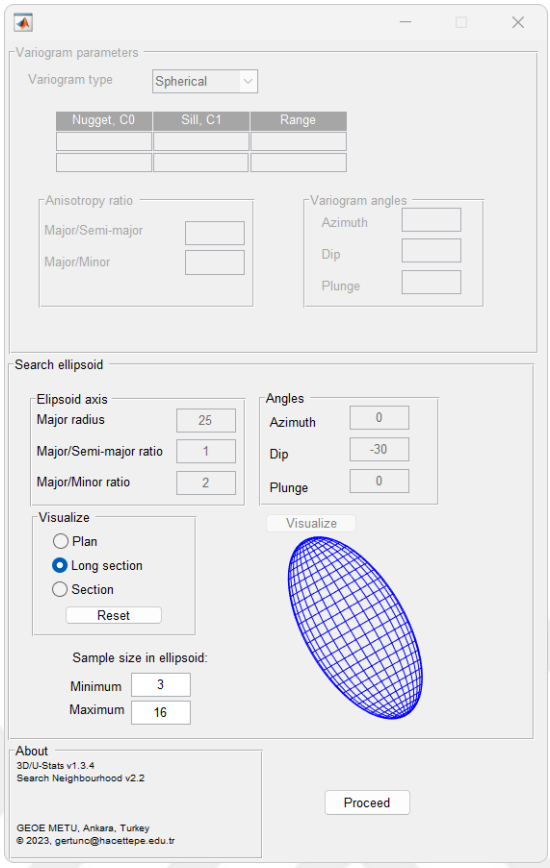
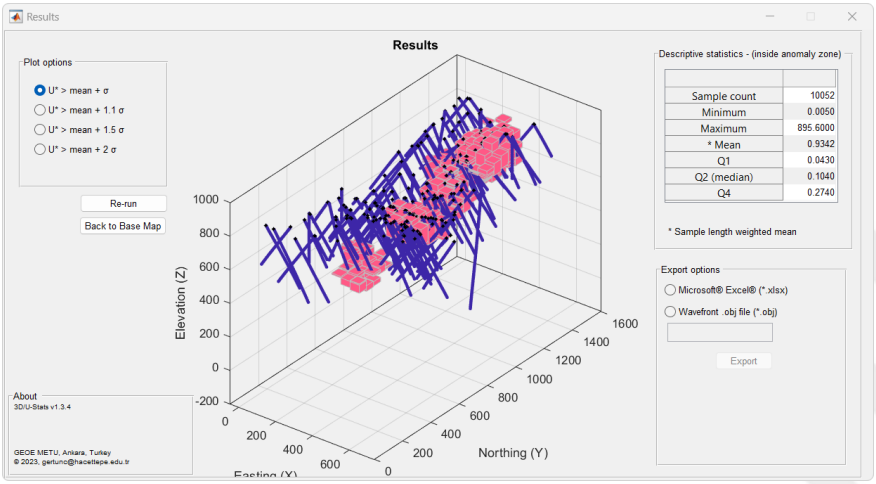
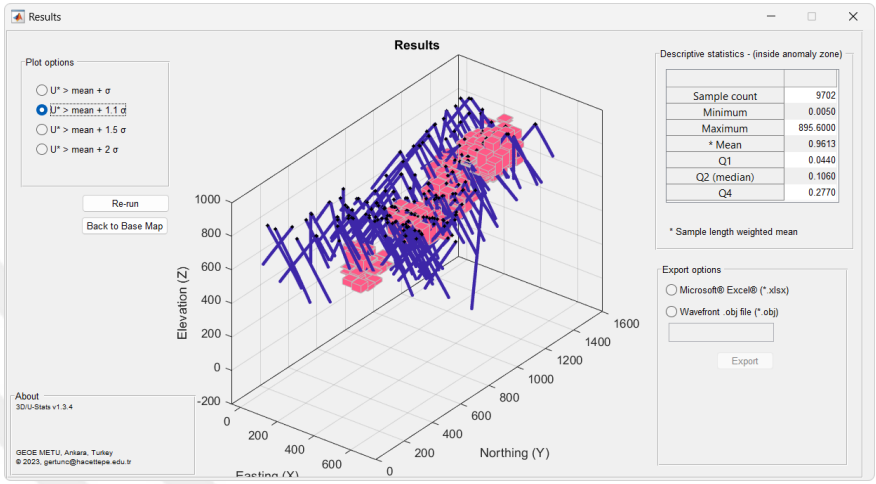


Figure 6.14: Taç search ellipsoid

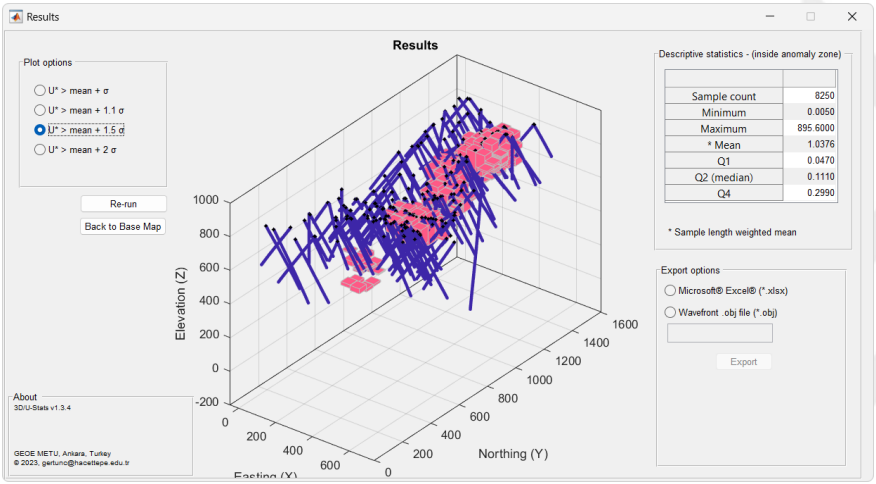
In Figure 6.15 binary maps of the Taç geochemical anomaly zone results are given. The results obtained according to different σ values' descriptive statistics are summarized in 6.3.



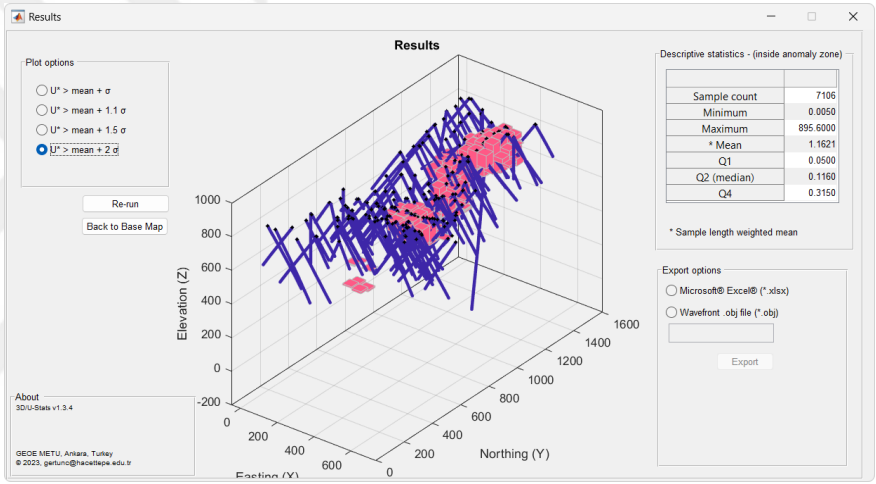
(a) mean(U^*) + σ



(b) mean(U^*) + 1.1 σ



(c) mean(U^*) + 1.5 σ



(d) mean(U^*) + 2 σ

Figure 6.15: U-Stats GUI: 3D, Taç results

Table 6.3: Results comparison of different multipliers of standard deviations in Taç mineralization

	U*>mean(U*) +			
	σ	1.1 σ	1.5 σ	2 σ
†Sample count	10052	9702	8250	7106
Minimum	0.005			
Maximum	895.6			
‡Mean	0.934	0.961	1.038	1.162
Q1	0.043	0.044	0.047	0.05
Q2 (median)	0.104	0.106	0.111	0.116
Q3	0.274	0.277	0.299	0.315

† samples fall inside 3D mesh grid

‡ length weighted

According to the statistical results of the raw data within the geochemical zone revealed by the different standard deviation multipliers of the Taç solutions, results were obtained such that the minimum and maximum values (0.005 and 895.6 ppm, respectively) were the same in all zones, as in the Salınbaş results. It can be seen that as the standard deviation multiplier increases, the length weighted mean, Q1, Q2, and Q3 values also increase, as expected.

CHAPTER 7

DISCUSSION, CONCLUSIONS, AND FUTURE WORK

In this thesis study, main focus was to determine geochemical anomaly zones from two different types of Au mineralizations using 3D U-Statistics. The main reason for choosing two different mineralization types is to test whether the results of the algorithm can reveal the differences of these distinct mineralization styles (vein-type epithermal versus carbonate-replacement type) and geochemical anomalies with different characteristics. At Taç, unlike the Salınbaş mineralization, the Au (ppm) attribute, which is within the alteration controlled units, was constrained and used. The reason for this is to emphasize the importance of including all possible geological information into the system, not only based on grade, in the statistical studies in exploration geochemistry.

Geometric comparison of the Taç and Salınbaş geochemical anomaly zones revealed that the Taç anomaly zone had a greater geological continuity in spite of using similar search ellipsoids, while the Salınbaş anomaly zone exhibited a clustered structure Figure 6.10 and 6.15). The cluster structure is in close agreement with geological studies performed in the field (Figure 6.11 and Groves et al., 2017). As for Taç mineralization, there exists a very strong correlation between the anomaly zone and the resource model (Ertunç et al., 2018).

In both Taç and Salınbaş projects, the 3D U-statistics output models show close correlation with their respective ore body distributions. Taç is an intermediate-sulfidation epithermal type mineralization that is largely hosted in narrow quartz-sulfide vein arrays. Such mineralized systems are generally developed in close association with steeply-dipping faults also commonly hosting the mineralized veins (Hedenquist et al., 2000, Simmons et al., 2005). At Taç, the output blocks of anomalous target areas

particularly show a vertical continuity in the northern part of the project area, near the Karsibayir Hill domain (Figure 6.15). However, the highlighted targets plunge gently towards south with a pronounced decrease in the lateral continuity. This is highly consistent with the previously established solid models of the Taç project (Barnett et al., 2011).

In Salınbaş, on the other hand, the output 3D U-statistics block model of geochemical Au anomalies has a dominant lateral component (as opposed to vertical). This is most likely due to the prominent control of the lithological contact between the Ziyarettepe limestone and the overlying Kizilcik Formation, which is a shallowly-dipping contact (Groves et al., 2017). Another important feature of the 3D U-Statistics model of the Salınbaş Hydrothermal project is that the geochemical anomaly blocks are rather sporadic and appear to be disconnected from one another (Fig). On possible explanation to this may be the irregular replacement style of mineralization, where ore minerals were precipitated within zones of carbonate dissolution and karstification.

Overall, it appears that distributions of geochemical anomalies at Taç and Salınbaş obtained through 3D U-statistics algorithm appear to reflect the mechanisms by which hydrothermal gold precipitation occurred in both sites.

When the anomaly zones of both mineralizations are compared statistically (Table 6.2 and 6.3), it can be concluded that the variation characteristics of the length weighted mean, Q1, Q2, and Q3 values according to different multipliers of standard deviations are also different. For the Taç, there is almost no variability in the Mean, Q1, Q2, and Q3 values. In Salınbaş, these values are in a more obvious increasing trend. This result can be interpreted as a natural consequence that the two different types of mineralization are different in terms of their anomaly structures as well as the grade continuity characteristics within the anomaly zones.

Mineral exploration activities are continuing in Salınbaş. In the light of U-Statistics results, it can be predicted that better planning of exploration drilling campaigns will be possible.

This version (v1.3.4) of U-Stats GUI only supports univariate cases. In the future releases, additional statistical tools for bivariate and/or multivariate cases will be im-

plemented. As a descriptive statistics tool, scatter plots and principal component analysis for the multidimensional data setups will be supported as well.

In this version, the search neighborhood parameters are only intuitively entered into the program. Determining the parameters of the search neighborhood with the aid of a tool for spatial continuity of geochemical anomalies will certainly improve the performance of geochemical anomaly mapping.

Another important spatial statistics feature variogram will also be an additional option in future releases. After variogram modelling, users will be available to set the search neighbourhood parameters accordingly.

In addition, before applying the U-Statistic method, it is recommended to determine the upper limit of the threshold value with methods used for outlier detection such as relative cumulative frequency curve, calculated distribution function, 4σ outlier test, and iterative 2σ techniques as well.

Swath plots represents changes in the mean value of attribute with respect to directions. In the next update of the software, this important spatial setting feature will be available.

REFERENCES

Afzal, P., Mirzaei, M., Yousefi, M., Adib, A., Khalajmasoumi, M., Zarifi, A. Z., Foster, P., & Yasrebi, A. B. (2016). Delineation of geochemical anomalies based on stream sediment data utilizing fractal modeling and staged factor analysis. *Journal of African Earth Sciences*, *119*, 139–149.

Arias, M., Gumiel, P., & Martín-Izard, A. (2012). Multifractal analysis of geochemical anomalies: A tool for assessing prospectivity at the se border of the ossa morena zone, variscan massif (spain). *Journal of Geochemical Exploration*, *122*, 101–112.

Asadi, H. H., Kianpouryan, S., Lu, Y.-J., & McCuaig, T. C. (2014). Exploratory data analysis and c–a fractal model applied in mapping multi-element soil anomalies for drilling: A case study from the sari gunay epithermal gold deposit, nw iran. *Journal of Geochemical Exploration*, *145*, 233–241.

Baize, D., & Sterckeman, T. (2001). Of the necessity of knowledge of the natural pedo-geochemical background content in the evaluation of the contamination of soils by trace elements. *The Science of the Total Environment*, *264*, 127–39.

Barnett, W., Doerksen, G., Murphy, B., Nowak, M., Pilotto, D., Rykaart, M., & Bonson, C. (2011). *Preliminary economic assessment on the taç and çorak deposits, yusufeli property, artvin province, turkey* [Report Prepared for Mediterranean Resources Ltd., SRK Consulting (Canada) Inc.].

Carranza, E. J. M. (2010). Catchment basin modelling of stream sediment anomalies revisited: Incorporation of eda and fractal analysis. *Geochemistry: Exploration, Environment, Analysis*, *10*(4), 365–381.

Carranza, E. J. M. (2008). *Geochemical anomaly and mineral prospectivity mapping in gis*. Elsevier.

Cheng, Q. (1999). Spatial and scaling modelling for geochemical anomaly separation. *Journal of Geochemical Exploration*, *65*(3), 175–194.

Cheng, Q., Agterberg, F., & Ballantyne, S. (1994). The separation of geochemical anomalies from background by fractal methods. *Journal of Geochemical Exploration*, *51*(2), 109–130.

Cheng, Q., Agterberg, F., & Bonham-Carter, G. (1996). A spatial analysis method for geochemical anomaly separation. *Journal of Geochemical Exploration*, *56*(3), 183–195.

Crommentuijn, T., Sijm, D., Bruijn, J., Van Leeuwen, K. V. L., & Plassche, E. (2000). Maximum permissible and negligible concentrations for some organic substances and pesticides. *Journal of Environmental Management*, *58*, 297–312.

Ertunç, G., İmer, A., Tercan, A. E., & Atalay, F. (2018). *Implicit modeling of hydrothermal mineral deposits with indicator kriging based support vector machines: Case study of taç altın and kurşunkaya iron deposits* [TUBITAK 1001 - The Scientific and Technological Research Projects Funding Program Final Report [In Turkish]].

Ertunç, G., & İmer, A. (2022). Minimum eğrilik algoritması ile yönlü sondaj ve kompozitleme bilgisayar programı, 615. https://hdl.handle.net/11511/96893

Ghannadpour, S. S., Hezarkhani, A., & Sabet-Mobarhan-Talab, A. (2017). The parkam exploration district, kerman, iran: Geology, ,alterations, and delineation of cu- and mo-mineralized zones using u-spatial statistic with associated software development. *Journal of Earth Science*, *28*(2), 283–294. https://doi.org/https://doi.org/10.1007/s12583-017-0722-z

Ghavami-Riabi, R., Seyedrahimi-Niaraq, M., Khalokakaie, R., & Hazareh, M. (2010). U-spatial statistic data modeled on a probability diagram for investigation of mineralization phases and exploration of shear zone gold deposits. *Journal of Geochemical Exploration*, *104*(1), 27–33. https://doi.org/https://doi.org/10.1016/j.gexplo.2009.10.002

Gonçalves, M. A., Mateus, A., & Oliveira, V. (2001). Geochemical anomaly separation by multifractal modelling. *Journal of Geochemical Exploration*, *72*(2), 91–114.

Groves, I., Coller, I. V., Mert, B., & White, S. (2017). *Geology and exploration potential of the artvin project, eastern pontides north eastern turkey* [Report Prepared for Ariana Resources].

Hao, L., Zhao, X., Zhao, Y., Lu, J., & Sun, L. (2014). Determination of the geochemical background and anomalies in areas with variable lithologies. *Journal of Geochemical Exploration*, *139*, 177–182.

Hedenquist, J. W., Arribas, A., & Gonzalez-Urien, E. (2000). Exploration for epithermal gold deposits. *Reviews in Economic Geology*, *13*, 45–77.

Horckmans, L., Rudy, S., Deckers, J., & Maquil, R. (2005). Local background concentrations of trace elements in soils: A case study in the grand duchy of luxembourg. *Catena*, *59*, 279–304.

Islam, M., & Hossain, M. (2021). Advances in directional drilling. In M. Islam & M. Hossain (Eds.), *Drilling engineering* (pp. 179–316). Gulf Professional Publishing.

Kandemir, Ö., Akbayram, K., Çobankaya, M., Kanar, F., Pehlivan, Ş., Tok, T., Hakyemez, A., Ekmekçi, E., Danacı, F., & Temiz, U. (2019). From arc evolution to arc-continent collision: Late Cretaceous–middle Eocene geology of the Eastern Pontides, northeastern Turkey. *GSA Bulletin*, *131*(11-12), 1889–1906.

Karsli, O., Dokuz, A., Uysal, I., Aydin, F., Chen, B., Kandemir, R., & Wijbrans, J. (2010). Relative contributions of crust and mantle to generation of Campanian high-K calc-alkaline I-type granitoids in a subduction setting, with special reference to the Harşit Pluton, Eastern Turkey. *Contributions to Mineralogy and Petrology*, *160*(4), 467–487.

Kuşcu, İ., Tosdal, R. M., & Gençalioğlu-Kuşcu, G. (2019). Episodic porphyry cu (-mo-au) formation and associated magmatic evolution in turkish tethyan collage. *Ore Geology Reviews*, *107*, 119–154.

Levinson, A. (1974). *Introduction to exploration geochemistry*. Apud Aedes Universitatis Gregorianae.

Li, C., Ma, T., & Shi, J. (2003). Application of a fractal method relating concentrations and distances for separation of geochemical anomalies from background. *Journal of Geochemical Exploration*, *77*(2), 167–175.

Luz, F., Mateus, A., Matos, J. X., & Goncalves, M. A. (2014). Cu- and zn-soil anomalies in the ne border of the south portuguese zone (iberian variscides, portugal) identified by multifractal and geostatistical analyses. *Natural resources research (New York, N.Y.)*

Matheron, G. (1971). In *The Theory of Regionalized Variables and Its Applications*. Les Cahiers du Centre de Morphologie Mathematique in Fontainebleau Paris.

Matschullat, J., Ottenstein, R., & Reimann, C. (2000). Geochemical background - can we calculate it? *Environmental Geology*, *39*, 990–1000.

Neuwirth, E. (2022). *Rcolorbrewer: Colorbrewer palettes* [R package version 1.1-3]. https://CRAN.R-project.org/package=RColorBrewer

Okay, A. I., & Şahintürk, Ö. (1997). Geology of the Eastern Pontides. In *Regional and Petroleum Geology of the Black Sea and Surrounding Region*. American Association of Petroleum Geologists.

Plumlee, G. S. (1997). The Environmental Geology of Mineral Deposits. In *The Environmental Geochemistry of Mineral Deposits: Part A: Processes, Techniques, and Health Issues Part B: Case Studies and Research Topics*. Society of Economic Geologists.

R Core Team. (2023). *R: A language and environment for statistical computing*. R Foundation for Statistical Computing. Vienna, Austria. https://www.R-project.org/

Rabayrol, F., Wainwright, A. J., Lee, R. G., Hart, C. J., Creaser, R. A., & Camacho, A. (2023). District-scale vms to porphyry-epithermal transitions in subduction to postcollisional tectonic environments: The artvin au-cu district and the hod gold corridor, eastern pontides belt, turkey. *Economic Geology*, *118*(4), 801–822.

Reimann, C., Filzmoser, P., & Garrett, R. G. (2005). Background and threshold: Critical comparison of methods of determination. *Science of The Total Environment*, *346*(1), 1–16.

Reimann, C., & Garrett, R. G. (2005). Geochemical background—concept and reality. *Science of The Total Environment*, *350*(1), 12–27.

Resources, A. (last visited on October 2023). https://doi.org/https://www.arianaresources.com/projects/zenit-madencilik/salinbas

Robinson, A. G., Banks, C. J., Rutherford, M. M., & Hirst, J. P. P. (1995). Stratigraphic and structural development of the Eastern Pontides, Turkey. *Journal of the Geological Society*, *152*(5), 861–872.

Rose, A., Hawkes, H., & Webb, J. (1979). *Geochemistry in mineral exploration*. Academic Press.

Sawaryn, S., & Thorogood, J. (2005). A compendium of directional calculations based on the minimum curvature method. *SPE Drilling & Completion*, *20*, 24–36. https://doi.org/10.2118/84246-PA

Simmons, S. F., White, N. C., & John, D. A. (2005). Geological Characteristics of Epithermal Precious and Base Metal Deposits. In *One Hundredth Anniversary Volume*. Society of Economic Geologists.

Topuz, G., Altherr, R., Schwarz, W. H., Siebel, W., Satır, M., & Dokuz, A. (2005). Post-collisional plutonism with adakite-like signatures: The eocene saraycık granodiorite (eastern pontides, turkey). *Contributions to Mineralogy and Petrology*, *150*(4), 441–455.

Wang, X., Xie, X., Cheng, Z., & Liu, D. (1999). Delineation of regional geochemical anomalies penetrating through thick cover in concealed terrains — a case history from the olympic dam deposit, australia. *Journal of Geochemical Exploration*, *66*(1), 85–97.

Yigit, O. (2009). Mineral Deposits of Turkey in Relation to Tethyan Metallogeny: Implications for Future Mineral Exploration. *Economic Geology*, *104*(1), 19–51.

Yilmaz, H. (2003). Geochemical exploration for gold in western turkey: Success and failure. *Journal of Geochemical Exploration*, *80*(1), 117–135.

Yilmaz, H., Sonmez, F. N., & Carranza, E. J. M. (2015). Discovery of au–ag mineralization by stream sediment and soil geochemical exploration in metamorphic terrain in western turkey. *Journal of Geochemical Exploration*, *158*, 55–73.

Yilmaz, H., Yousefi, M., Parsa, M., Sonmez, F. N., & Maghsoodi, A. (2019). Singularity mapping of bulk leach extractable gold and 80 stream sediment geochemical data in recognition of gold and base metal mineralization footprints in biga peninsula south, turkey. *Journal of African Earth Sciences*, *153*, 156–172.